Conformality of atomic layer deposition in microchannels: impact of process parameters on the simulated thickness profile

Authors: Jihong Yim,[1]* Emma Verkama,[1]* Jorge A. Velasco,[1] Karsten Arts,[2] and Riikka L. Puurunen[1]**

*These authors contributed equally

** Corresponding author: riikka.puurunen@aalto.fi

[1]Department of Chemical and Metallurgical Engineering, Aalto University, P.O. Box 16100, FI-00076 AALTO, Finland

[2]Department of Applied Physics, Eindhoven University of Technology, P.O. Box 513, 5600 MB Eindhoven, The Netherlands

Keywords: atomic layer deposition, conformality, high-aspect-ratio, diffusion-reaction model, sticking coefficient, simulation

ABSTRACT

Unparalleled conformality is driving ever new applications for atomic layer deposition (ALD), a thin film growth method based on repeated self-terminating gas-solid reactions. In this work, we re-implemented a diffusion-reaction model from the literature to simulate the propagation of film growth in wide microchannels and used that model to explore trends in both the thickness profile as a function of process parameters and different diffusion regimes. In the model, partial pressure of ALD reactant was analytically approximated. Simulations were made as function of kinetic and process parameters such as temperature, (lumped) sticking coefficient, molar mass of the ALD reactant, reactant's exposure time and pressure, total pressure, density of the grown material, and growth per cycle (GPC) of the ALD process. Increasing the molar mass and the GPC, for example, resulted in a decreasing penetration depth into the microchannel. The influence of the mass and size of the inert gas molecules on the thickness profile depended on the diffusion regime (free molecular flow vs. transition flow). The modelling was compared to a recent slope method to extract the sticking coefficient. The slope method gave systematically somewhat higher sticking coefficient values compared to the input sticking coefficient values; potential reasons behind the observed differences are discussed.

1. Introduction

Unparalleled conformality is driving ever new applications for atomic layer deposition (ALD), a thin film growth method based on repeated self-terminating gas-solid reactions.[1–3] ALD enables one to make conformal coatings on almost any desired inorganic substrate including high aspect ratio (HAR) structures such as microelectronics and powder media. Yet, tuning of the process parameters is often required to guarantee conformal coatings in HAR structures.

Several types of feature-scale models have been used to simulate ALD growth in high aspect ratio (HAR) structures [e.g. Figure 1(a)], as recently reviewed by Cremers et al.[4] Analogously to a recent article on chemical vapor deposition,[5] we classify these ALD models as ballistic line-of-sight (e.g. refs. 6–9), Monte Carlo (e.g. refs. 10–17) and diffusion-reaction models (e.g. refs. 18–22).‡ While the heterogeneous gas–solid reactions responsible for ALD growth have been demonstrated at a great range of pressures from atmospheric to ultra-high vacuum,[4,17,23] ALD processes often operate in a low vacuum of roughly 10^2 Pa range.[3] Consequently, most feature-scale models for ALD have been developed for low-pressure conditions where the mean-free-path of the molecules λ is much higher than the limiting dimension of the feature h (Knudsen number $Kn = \lambda/h >> 1$).[9,24] Here, molecules collide with the feature walls and not with other molecules in the gas phase, and the mass transport regime is referred to as varied names e.g. as (free) molecular flow, Knudsen flow, or Knudsen diffusion.[4,19,25,26] Diffusion-reaction models based on Fick's law of diffusion can flexibly be used in free molecular flow ($Kn >> 1$) as well as in transition flow ($Kn \approx 1$) and even in

‡ Diffusion-reaction models relying on Fick's laws of diffusion are in the ALD literature sometimes somewhat confusingly referred to as "continuum" models;[4,30,33] in this work the term is dedicated to continuum flow conditions where the mean free path of molecules λ (m) is orders of magnitude smaller than the limiting feature dimension h (m) (Knudsen number $Kn = \lambda/h \leq 10^{-3}$).[25]

50 continuum flow (*Kn* << 1) conditions,[24,26,27] as the effective diffusion coefficient D_{eff} ($m^{-2}s^{-1}$)
51 can be calculated from the gas-phase diffusion coefficient D_A ($m^{-2}s^{-1}$) and the Knudsen
52 diffusion coefficient D_{Kn} ($m^{-2}\,s^{-1}$).[17,18,20] Also Monte Carlo methods have been used for regimes
53 other than free molecular flow, by using the mean free path λ as a statistical parameter.[11–13]
54 Irrespective of the theoretical framework, all models reproduce the typical profiles of ideal
55 ALD growth based on self-terminating (i.e., saturating and irreversible) reactions:[3,28] constant
56 film thickness followed by an abrupt decrease to zero, as illustrated in Figure 1(b).

57 For ALD process modelling and reactor design, a useful description of the
58 reaction kinetics is essential. Typically, the reaction kinetics of ALD processes are described in
59 a simplified manner assuming irreversible single-site Langmuir adsorption and an associated
60 (lumped) sticking coefficient.[4,7,13,17,20,29] Experimental knowledge of sticking coefficients has
61 been rather scarce until recently.[4,7,8,11,12,29–31] The most straightforward way of analysing the
62 kinetics is by interpreting film termination profiles measured in dedicated test structures or
63 in a cross-flow reactor, where a steep film termination profile is generally associated with
64 high reactivity.[11,12,29,30,32,33]

65 Recently, microscopic lateral high-aspect-ratio (LHAR) test channels have
66 emerged for thickness profile measurements.[18,34–36] Such LHAR structures simplify
67 conformality analysis: after ALD, the roof of the structure can be removed, exposing the film
68 to detailed analysis.[35–37] Further, a method has been developed by Arts et al.[30] to be used in
69 conjunction with microscopic LHAR test channels, where the sticking coefficient *c* can be
70 calculated from the slope [at surface coverage θ (-) of 1/2] of the Type 1 normalized thickness
71 profile [Figure 1(b)] through a simple square root relation.[30] This *slope method* was derived

empirically from the diffusion-reaction model of Yanguas-Gil and Elam at free molecular flow conditions.[20]

In this work, we have re-implemented the diffusion–reaction model by Ylilammi et al.[18] and used it to simulate the evolution of ALD growth at various scenarios of kinetic and process parameters and diffusion regimes. We first describe the assumptions and equations behind the Ylilammi et al.[18] diffusion-equation model. We then demonstrate how process parameters influence the ALD thickness profile by varying individual parameters at various diffusion regimes and channel filling levels. Finally, we compare the simulations of the Ylilammi et al.[18] model with the Arts et al.[30] slope method and discuss the likely reasons for the observed slight differences.

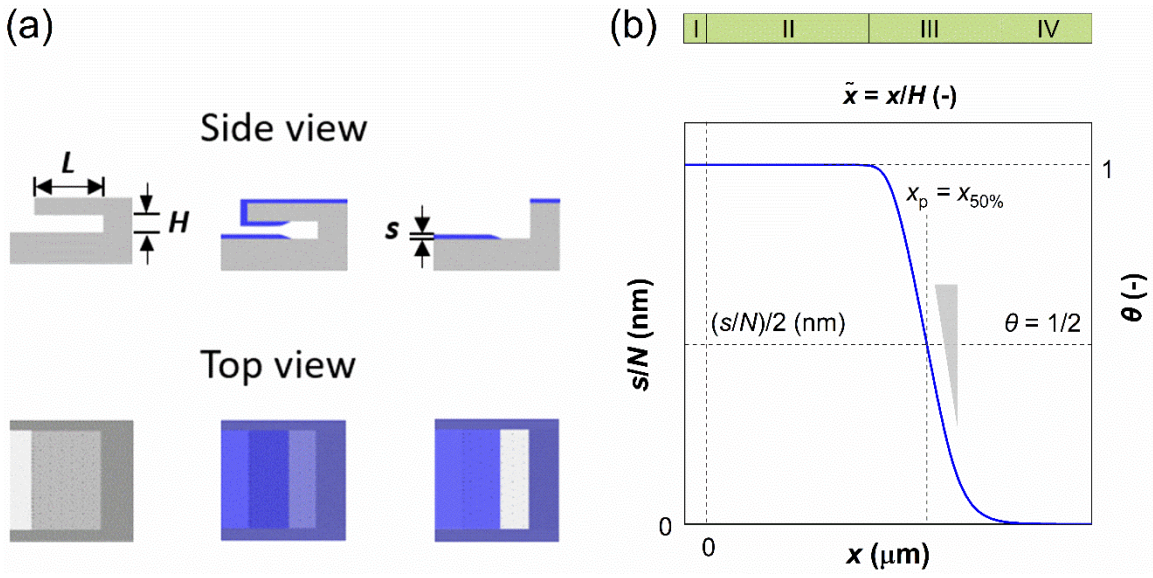

Figure 1. Illustration of ALD film in wide microchannel structures: (a) side and top views of the microchannel with length *L* and height *H*, containing a film with thickness *s* at the channel entrance (illustration intentionally not to scale). (b) Illustration of the different regions (I-IV) of a thickness profile superimposed on a thickness profile with different axes

shown. The classifications of thickness profiles and the regions are as in ref. 36, except that here we use the term *thickness profile* instead of *saturation profile*.

2. Description of the Ylilammi et al.[18] diffusion-reaction model

For full details behind the model derivation, please see the article by Ylilammi et al.[18] Here, core concepts are presented that are used in the current implementation. In some cases, somewhat expanded explanations are provided, to help the reader follow the model and connect it to other models on ALD.

2.1. Basic ALD process and geometry assumptions

The Ylilammi et al.[18] model was built to describe a typical ALD process, based on the use of inert gas for transporting the reactant from the source to the growth surface.[3]

The considered high-aspect-ratio (HAR) geometry is a wide microchannel similar to the one in Figure 1(a), where height H (m) of the microchannel is the limiting dimension. The width W (m) of the microchannel is orders of magnitude larger than H, and the length L (m) is considered infinite (the channel end effects are not considered). While the model has been constructed with lateral HAR (LHAR) structures in mind,[35,36] it is indifferent to the orientation of the structure and thus describes vertical trenches (and any other orientation) as well.

Typically, an ALD process has at least two reactants, often called Reactant A and Reactant B.[3] In this model, one of the two reactions is assumed to limit the extent of film growth in the microchannel; typically, this is assumed to be the reaction of Reactant A. The partial pressure of Reactant A is denoted as p_A (Pa). Reactant A is brought to the microchannel entrance at a partial pressure p_{A0}.[18] It is expected that the partial pressure of Reactant A

behaves like a step function: during the reactant pulse, the pressure at the microchannel entrance is p_{A0}, and otherwise it is zero.[3,38] An inert carrier gas, denoted here with "I" (instead of the notation "B" used in the Ylilammi et al.[18] article, to avoid confusion with Reactant B[3]), is used to aid the transport of Reactant A from the source to the surface. The inert gas has the same partial pressure p_I (Pa) inside and outside of the microchannel. Inside the microchannel, p_A decreases, as Reactant A is consumed in the adsorption (i.e., ALD) process. The time t from the beginning (t = 0) until the end of exposure of Reactant A (t = t_1) is considered; purge is excluded from this model. Thus, of the four typical steps in an ALD sequence,[3] the current simulation concerns Step 1 only.

2.2. Mass transport by diffusion and partial pressure of Reactant A

In the chosen geometry, the partial pressure of Reactant A can be considered constant in the y- and z- direction.[18] The one-dimensional diffusion equation for the partial pressure of Reactant A p_A (Eq. 10 of Ylilammi et al.[18]) is:

$$\frac{\partial p_{\mathrm{A}}}{\partial t} = D_{\mathrm{eff}} \frac{\partial^2 p_{\mathrm{A}}}{\partial x^2} - \frac{4gRT}{hN_0}. \quad (1)$$

The second term on the right side of this equation is called the *adsorption loss* term. R is the gas constant (8.314461 J K^{-1} mol^{-1}), T is the absolute temperature (K), and N_0 is Avogadro's constant (mol^{-1}). The effective diffusion coefficient D_{eff} considers both the gas-phase collisions and the channel wall collisions through the gas-phase diffusion coefficient D_A (m^2 s^{-1}), as well as the Knudsen diffusion coefficient D_{Kn} (m^2 s^{-1}), in the Bosanquet relation (Eq. 6 of Ylilammi et al.[18]):

$$D_{\mathrm{eff}} = \frac{1}{\frac{1}{D_{\mathrm{A}}} + \frac{1}{D_{\mathrm{Kn}}}}. \quad (2)$$

In Eq. 1, g (m^{-2} s^{-1}) is the net adsorption rate of molecules from the gas phase to the surface. h (m) is the hydraulic diameter of the microchannel (Eq. 5 of Ylilammi et al.[18]):

$$h = \frac{2}{\frac{1}{H} + \frac{1}{W}}. \tag{3}$$

The gas-phase diffusion coefficient depends on the average speed of the Reactant A molecules $\bar{v}_\mathrm{A}$ (m s^{-1}) and the collision rate of the Reactant A molecules in a mixture of A and B, z_A (s^{-1}) (Eq. 3, Ylilammi et al.[18]):

$$D_\mathrm{A} = \frac{3\pi {\bar{v}_\mathrm{A}}^2}{16 z_\mathrm{A}}. \tag{4}$$

The average speed of molecules A (i.e. the thermal velocity) is, from the kinetic theory of gases, obtained as (Eq. 2 of Ylilammi et al.[18]):

$$\bar{v}_A = \left(\frac{8RT}{\pi M_\mathrm{A}}\right)^{\frac{1}{2}}. \tag{5}$$

The collision frequency of molecules A in a mixture of A and inert gas I is, from the kinetic theory of gases, obtained as (Eq. 1, Ylilammi et al.[18]):

$$z_\mathrm{A} = \frac{\pi}{4}(d_\mathrm{A} + d_\mathrm{I})^2 \left[\frac{8RT}{\pi}\left(\frac{1}{M_\mathrm{A}} + \frac{1}{M_\mathrm{I}}\right)\right]^{\frac{1}{2}} \frac{p_\mathrm{I} N_0}{RT} + \pi (d_\mathrm{A})^2 \left[\frac{16RT}{\pi M_\mathrm{A}}\right]^{\frac{1}{2}} \frac{p_\mathrm{A} N_0}{RT}. \tag{6}$$

Here, d_A and d_I are the (hard-sphere model) diameters (m) of molecules A and the inert gas, respectively, and M_I is the molar mass of the inert gas (g mol^{-1}).[§] The diameters can be

[§] Note that Eq. 1 of Ylilammi et al.[18] for calculating the collision frequency contains an error:[36] both terms on the right side of Eq. 1 of ref. 18 have been multiplied by Avogadro's number for Eq. 6 of this work.

estimated for example from the gas-phase viscosity (Eq. 7 of Ylilammi et al.[18]) or the liquid phase density (Eq. 8 of Ylilammi et al.[18]).

The Knudsen diffusion coefficient D_{Kn} depends on the microchannel's hydraulic diameter h, the temperature T, and the molar mass of Reactant A, M_{A} (kg mol^{-1}) (Eq. 4 of Ylilammi et al.[18]):

$$D_{\mathrm{Kn}} = h\left(\frac{8RT}{9\pi M_{\mathrm{A}}}\right)^{\frac{1}{2}}. \tag{7}$$

Instead of solving the differential equation for the partial pressure of Reactant A (Eq. 10 of Ylilammi et al.[18]) numerically, Ylilammi et al.[18] derived an approximate analytic solution of the diffusion equation, which is implemented in this work. With the approximate solution, the partial pressure of Reactant A p_{A} can be analytically calculated for any position x and time t. In the part of the profile where the net adsorption rate g is approximately zero ($x < x_{\mathrm{t}}$, where t stands for "transition"), the partial pressure p_{A} decreases linearly with x (Eq. 18 of Ylilammi et al.[18]) (Figure S1):

$$p_{\mathrm{A}}(x,t) = p_{\mathrm{A0}}\left(1 - \frac{x}{x_{\mathrm{s}}}\right), \qquad x < x_{\mathrm{t}}, \tag{8}$$

And beyond the point $x = x_{\mathrm{t}}$, the decrease is exponential (Eq. 24 of Ylilammi et al.[18]):

$$\begin{aligned} p_{\mathrm{A}}(x,t) &= p_{\mathrm{At}} \exp\left(-\frac{x - x_{\mathrm{t}}}{x_{\mathrm{s}} - x_{\mathrm{t}}}\right), \qquad x > x_{\mathrm{t}}, \\ p_{\mathrm{At}} &= p_{\mathrm{A0}}\left(1 - \frac{x_{\mathrm{t}}}{x_{\mathrm{s}}}\right). \end{aligned} \tag{9}$$

In Eqs. 8 and 9, x_{s}, where the linearly extrapolated partial pressure p_{A} is zero, is obtained from (Eq. 19, Ylilammi et al.[18]):

$$x_{\mathrm{s}} = \sqrt{Dt}. \tag{10}$$

Here, D is the apparent longitudinal diffusion coefficient ($m^2\ s^{-1}$), which is obtained from (Eq. 23, Ylilammi et al.[18]):

$$D = \frac{p_{\mathrm{A0}} H D_{\mathrm{eff}}}{q k_B T \left(1 - \frac{\ln(K p_{\mathrm{A0}} + 1)}{K p_{\mathrm{A0}}}\right)}. \tag{11}$$

Here, q is the adsorption density of the metal M atoms in the growth of film of the M_yZ_x material (m^{-2}) (i.e., the growth per cycle in ALD, expressed as areal number density), which can be calculated from the thickness-based growth per cycle (GPC) of the ALD process gpc_{sat} (Eq. 9, Ylilammi et al.[18]):

$$q = \frac{b_{\mathrm{film}}}{b_{\mathrm{A}}} \frac{\rho g p c_{\mathrm{sat}}}{M} N_0. \tag{12}$$

Here, b_{film} is the number of metal atoms in a formula unit of the growing film (e.g., 2 for Al_2O_3), b_{A} is the number of metal atoms in a Reactant A molecule (e.g., 1 for trimethylaluminium), ρ ($kg\ m^{-3}$) is the mass density of the ALD film material (composition denoted here as M_yZ_x), gpc_{sat} (m) is the ALD GPC (corresponding to saturated reactions) in thickness units, M ($kg\ mol^{-1}$) is the molar mass of one formula unit of the growing film (M_yZ_x), and N_0 is Avogadro's constant (mol^{-1}). The transition point x_{t} from Eq. 8 to Eq. 9 occurs at (Eq. 28, Ylilammi et al.[18]):

$$x_{\mathrm{t}} = x_{\mathrm{s}} - \sqrt{\frac{h N_0 D_{\mathrm{eff}}}{4 R T c Q}}, \qquad \text{if } x_s > \sqrt{\frac{h N_0 D_{\mathrm{eff}}}{4 R T c Q}}$$

$$x_{\mathrm{t}} = 0, \qquad \text{otherwise.} \tag{13}$$

Here, c is the sticking probability of Reactant A in collision with the microchannel wall ($0 \leq c \leq 1$, unitless). Q is the wall-collision rate at unit pressure ($m^{-2}\ s^{-1}\ Pa^{-1}$), calculated from (Eq. 14 of Ylilammi et al.[18]):

$$Q = \frac{N_0}{\sqrt{2\pi M_A RT}}. \quad (14)$$

In this model implementation, the gas-phase diffusion coefficient D_A is updated for all positions and times in each cycle, as D_A depends on the partial pressure of Reactant A p_A (x,t). The apparent longitudinal diffusion coefficient D and the effective diffusion coefficient D_{eff} are also updated accordingly, as they are influenced by the gas-phase diffusion coefficient D_A.

An illustration of how the partial pressure of Reactant A decreases inside the microchannel is shown in Figure 2(a). Simulation conditions similar to those of Ylilammi et al.[18] were used. Figure 2(a) shows a similar trend as Fig. 2 in Ylilammi et al.,[18] suggesting that the model was correctly re-implemented.

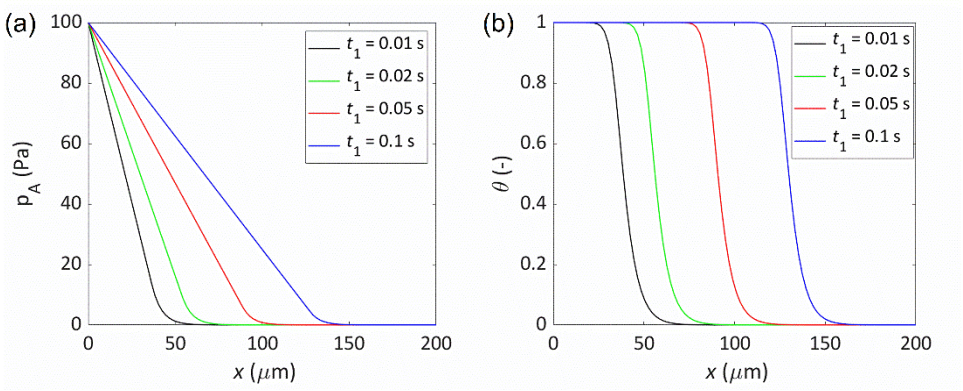

Figure 2. Illustration of the simulated parameters inside the microchannel as a function of location and time: (a) partial pressure of Reactant A, and (b) surface coverage. The figures correspond to Figs. 2 and 3 of Ylilammi et al.,[18] respectively. Parameters: c = 0.01, T = 523.15 K, p_{A0} = 100 Pa, M_A=0.0749 kgmol^{-1}, d_A = 5.91 × 10^{-10} m, p_I = 300 Pa, M_I = 0.028 kgmol^{-1}, d_I = 3.74 × 10^{-10} m, ρ = 3500 kgm^{-3}, gpc_{sat} = 1.06 × 10^{-10} m, K = 100 Pa^{-1}, q = 5 × 10^{18} m^{-2}, H = 500 nm, and W = 0.1 mm.

2.3. Langmuir adsorption model and surface coverage

The model is built on the assumption of reversible single-site Langmuir adsorption describing the gas-solid reaction step in ALD:[18]

$$\mathrm{A} + * \rightleftharpoons \mathrm{A}*. \tag{15}$$

Here, A is the reactant molecule, * is a surface site, and A* denotes a molecule adsorbed on a site. In the Langmuir adsorption model, a surface consisting of a checkerboard can be imagined: all sites are equal, and the adsorbed species are assumed to not interact with each other. If an elementary reaction was assumed, Eq. 15 would correspond on the assumption of an associative adsorption mechanism.[3] However, it is acknowledged that the actual surface reactions are more complex,[18] and in the model, Eq. 15 does not describe an elementary reaction but rather a lumped reaction.

The fraction of occupied adsorption sites is called the *surface coverage* and is denoted with θ ($0 \leq \theta \leq 1$). The fraction of unoccupied or vacant adsorption sites is $1 - \theta$. The rate of adsorption per unit surface area f_{ads} ($\mathrm{m^{-2}\ s^{-1}}$) is proportional to the fraction of vacant sites, the probability that a collision leads to adsorption c, and the frequency of collisions p_{A}, either as (Eq. 11, Ylilammi et al.[18]):

$$f_{\mathrm{ads}} = \frac{(1-\theta)cN_0 p_{\mathrm{A}}}{\sqrt{2\pi M_{\mathrm{A}} RT}}, \tag{16}$$

or through the use of the concept of the (gas-phase) collision rate at unit pressure Q:

$$f_{\mathrm{ads}} = (1-\theta)cQp_{\mathrm{A}}. \tag{17}$$

The rate of desorption f_{des} ($\mathrm{m^{-2}\ s^{-1}}$) depends on the surface concentration of the adsorbed species (θq, $\mathrm{m^{-2}}$) and the desorption probability in unit time P_{d} ($\mathrm{s^{-1}}$) (Eq. 12, Ylilammi et al.[18]):

$$f_{\mathrm{des}} = \theta q P_{\mathrm{d}}. \tag{18}$$

The net adsorption rate g (m^{-2} s^{-1}) is (Eq. 15, Ylilammi et al.[18])

$$g = f_{\mathrm{ads}} - f_{\mathrm{des}}. \tag{19}$$

At equilibrium, the net adsorption rate would be zero, the surface coverage would have reached the equilibrium value θ_{eq}, and the equilibrium constant can be defined as (Eq. 13, Ylilammi et al.[18]):

$$K = \frac{\theta_{\mathrm{eq}}/p_{\mathrm{A}}}{1-\theta_{\mathrm{eq}}} = \frac{f_{\mathrm{ads}}}{f_{\mathrm{des}}} = \frac{cQ}{qP_d}. \tag{20}$$

During adsorption, the ALD reactions are generally not at equilibrium, and the surface coverage θ is a function of x and time t. In the model, the surface coverage is solved numerically from the rate equation describing the rate of change of the surface coverage with time (Eq. 31, Ylilammi et al.[18]):

$$\frac{d\theta(x,t)}{dt} = \frac{cQp_{\mathrm{A}}(x,t)}{q} - \left(\frac{cQp_{\mathrm{A}}(x,t)}{q} + P_{\mathrm{d}}\right)\theta(x,t). \tag{21}$$

The solution requires the partial pressure of Reactant A as a function of position and time, for which Eqs. 8 and 9 are used.

An illustration of the surface coverage inside the microchannel is shown in Figure 2 (b). This figure shows a similar trend to Fig. 3 by Ylilammi et al.,[18] indicating that the model has been correctly re-implemented.

2.4. Effect of cycles on film thickness and parameters such as narrowing of the channel

For each cycle, the surface coverage profile is calculated separately, as in Eq. 21. The thickness increment caused by the surface coverage is (Eq. 37, Ylilammi et al.[18]):

$$s(x) = \theta(x) gpc_{\mathrm{sat}}. \tag{22}$$

In calculating the thickness profile *s*(*x*, *N*), the thickness increments caused by the *N* cycles are summed up:

$$s(x, N) = \sum_{i=1}^{N} \theta_i(x)\, gpc_{\mathrm{sat}}. \tag{23}$$

In the Ylilammi et al. model,[18] a simplification is made to assume that the free height of the microchannel *H* is decreases in each cycle by twice the GPC value, as film grows both on top and bottom of the microchannel (Eq. 35, Ylilammi et al.[18]):

$$H(N) = H(0) - 2N gpc_{\mathrm{sat}}. \tag{24}$$

The constant free channel height simplification increases the computational speed.[18] The consequence is that the surface coverage for an individual cycle decreases somewhat too steeply in Region III of the thickness profile [see Figure 1 (b)]. Ylilammi et al.[18] estimated that the assumption is valid when the film is thin compared to the height of the microchannel *H* and when the film does not grow much beyond the half-thickness penetration depth $x_{50\%}$ (x_{p} in the Ylilammi et al.[18] model).[18] An illustration of the simulated thickness profiles after 1000 cycles in microchannels with various heights is shown in Figure S2. Here, a similar trend is observed as that in Fig. 4 by Ylilammi et al.,[18] confirming that the model has been re-implemented properly. In this implementation, the Knudsen diffusion coefficient D_{Kn} is

updated from cycle to cycle as free height of the microchannel $H(N)$ is updated in each cycle (Eq. 7).

3. Experimental

3.1. Model implementation in MATLAB®

In this work, we used two different diffusion-reaction models by Ylilammi et al.[18] (Model A) and Yanguas-Gil and Elam[20] (Model B) to simulate ALD thickness profiles in LHAR.

3.1.1. Ylilammi et al.[18] model (Model A)

The resulting set of equations for surface coverage θ, reactant partial pressure p_A, and film thickness s along the microchannel was solved using the software MATLAB®. For discretisation of the geometric domain along the microchannel (x-axis), an equidistant array was used. Based on this, the temporal evolution of the surface coverage $\theta\ (x,t)$ (Eq. 21) was solved numerically by using MATLAB's ODE23 ordinary differential equation solver with a relative tolerance of 10^{-3} and an absolute tolerance of 10^{-5}. A simplified flowchart of the algorithm is shown in Figure 3. The temporal evolution of the reactant partial pressure (p_A) was calculated using Eqs. 8 and 9. To perform these calculations, it was assumed that p_A was zero along the entire microchannel when t = 0. The transport properties (i.e. D_{eff} and D) required for obtaining x_s and x_t (Eqs. 10 and 13, respectively) were computed for each element along the microchannel using the reactant partial pressure from the previous time step.*

The surface coverage profile $\theta(x,t)$ was computed by solving Eq. 21 until the target pulse time was reached. The film thickness profile $s(x)$ was obtained from Eq. 22 while the

* Earlier reports re-implemented the Ylilammi et al.[18] model to simulate the growth of aluminium oxide from trimethylaluminium (TMA) and water in wide microchannels.[18,36]

277 thickness increment and the updated microchannel height were calculated from Eq. 23 and
278 24, respectively. The previous procedure was repeated until the defined number of cycles (*N*)
279 was achieved.

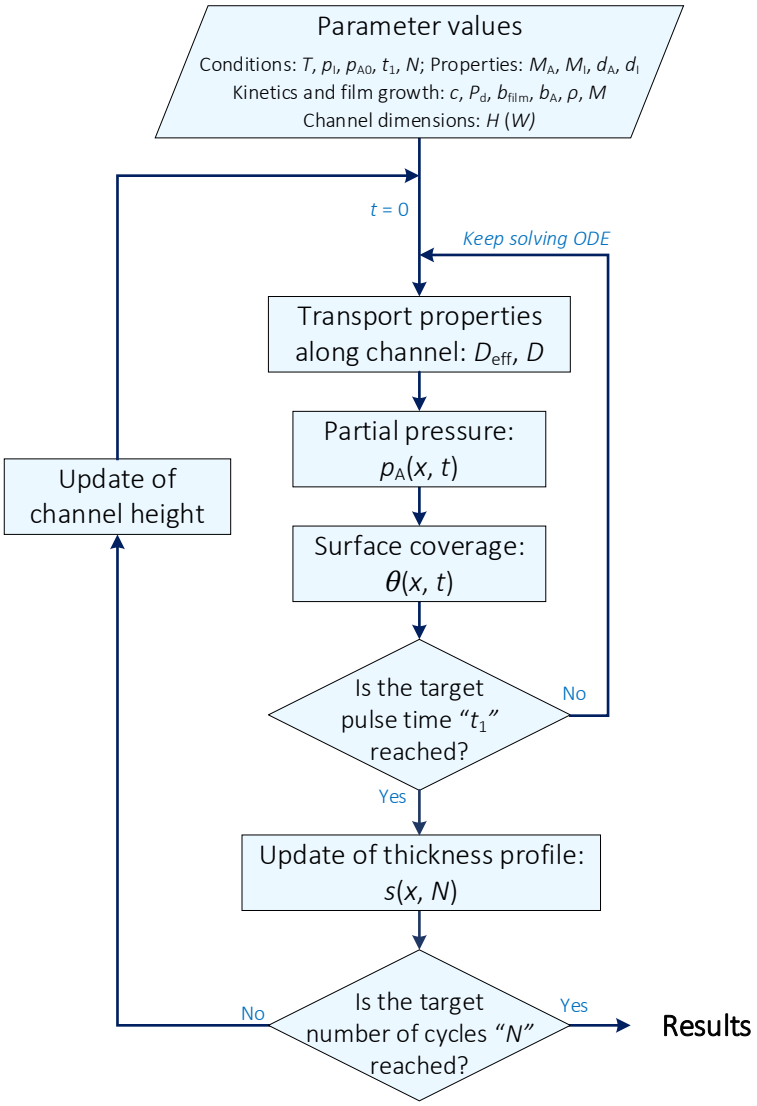

280

281 *Figure 3. Simplified algorithm for the simulation of thickness profiles with the re-implemented*
282 *Ylilammi et al.*[18] *diffusion-reaction model.*

283 ### 3.1.2. Yanguas-Gil and Elam[20] model (Model B)

284 The *slope method* reported by Arts et al.,[30] which is used to back-extract the
285 value of the (lumped) sticking coefficient, is based on the diffusion-reaction model reported

by Yanguas-Gil and Elam.[20] This model is similar to the Ylilammi et al. model,[18] but with three main differences. First, the Yanguas-Gil and Elam model[20] does not use a desorption term to calculate the evolution in θ, i.e., $P_d = 0$ in Eq. 21. Second, it assumes free molecular flow, i.e., $D_{eff} = D_{Kn}$. Third, it calculates the partial pressure directly from Eq. 1, by numerically solving the coupled equations for p_{A} (Eq. 1) and θ (Eq. 21) simultaneously. In this work, and in the work of Arts et al.[30] reporting on the *slope method*,[30] the coupled equations of the Yanguas-Gil and Elam model[20] were solved using MATLAB's pdepe solver.[39] This function solves a system of parabolic and elliptic partial differential equations with one spatial parameter (here, the distance x) and one time parameter t. For the implementation of Model B, the symmetry of the problem was set to 0, corresponding to slab geometry, and default tolerance values of 10^{-3} relative tolerance and 10^{-6} absolute tolerance were used. Analogous to the implementation of Model A, the parameters x and t were discretised using constant spacing. Finally, the initial conditions $p_{\mathrm{A}}(x,0) = 0$ and $\theta(x,0) = 0$ were used, in combination with the boundary conditions $p_{\mathrm{A}}(0,t) = p_{\mathrm{A0}}$ and $\frac{\partial p_{\mathrm{A}}}{\partial x}(L,t) = -\frac{1}{4}\frac{\bar{v}_{\mathrm{A}}}{D_{Kn}} c \cdot p(L,t)\big(1-\theta(L,t)\big)$.[20]

3.2. Simulation details

Simulations were made with MATLAB® scripts by varying an individual parameter while keeping other parameters constant. To extract the half-thickness penetration depth, the script chose the first point (x_i,y_i), where x_i is equal to or smaller than the half-thickness penetration depth, and then chose another discretisation point (x_{i-1},y_{i-1}), which was one point before (x_i,y_i). Once the two discretisation points were chosen, the half-thickness penetration depth and the slope at half-thickness penetration depth were interpolated linearly between the two discretisation points (see Figure S3). The total number

of discretisation points were selected so that the difference between those two discretisation points in *y*-axis is less than or equal to 3% of the whole range.

To compare the simulations made with the Ylilammi et al. model [18] and the Yanguas-Gil and Elam model,[20] and to back-extract the sticking coefficient by the slope method,[30] we chose conditions with $Kn \geq 100$.[9,20,24] The Knudsen number was calculated as (Eq. 1, Cremers et al.[4])

$$Kn = \frac{\lambda}{h}, \tag{25}$$

where λ (m) is the mean free path, and h (m) is the hydraulic diameter of the microchannel (Eq. 3).

The mean free path λ was calculated as (Eq. 3, Cremers et al.,[4] and Eq. 5.21,3 Chapman and Cowling[40]):

$$\lambda = \frac{k_B T}{\sqrt{2} p_{\mathrm{A}0} \sigma_{\mathrm{A,A}} + \sqrt{1 + \frac{m_{\mathrm{A}}}{m_{\mathrm{I}}}} p_{\mathrm{I}} \sigma_{\mathrm{A,I}}}, \tag{26}$$

where k_B (m^2 kg s^{-2} K^{-1}) is the Boltzmann constant, T (K) is the temperature, p_{I} (Pa) is the partial pressure of the inert gas I, $p_{\mathrm{A}0}$ is the partial pressure of Reactant A at the microchannel entrance (0,t), m_{I} (kg) is the mass of the inert gas molecule I, and $\sigma_{\mathrm{A,I}}$ (m^2) is the collision cross section between Reactant A and the inert gas I. The collision cross section between molecules i and j is calculated using the following equation (Eq.4, Cremers et al. [4]):

$$\sigma_{i,j} = \pi \left(\frac{d_i}{2} + \frac{d_j}{2} \right)^2, \tag{27}$$

where d_i (m) is the hard-sphere diameter of molecule *i.* [**] The excess number γ, which refers to the amount of Reactant A existing per adsorption site in the LHAR structure,[18] is calculated by using the following equation (Eq. 6 Yanguas-Gil and Elam[20]):

$$\gamma = \frac{V n_{\mathrm{A}}}{qS}, \tag{28}$$

where V (m^3) and S (m^2) are the volume and surface area of the HAR structure, respectively, q (m^{-2}) is the adsorption density, and n_{A} is the particle concentration (number density) of Reactant A (m^{-3}) at the microchannel entrance (0,*t*). We simulated thickness profiles at conditions where excess number γ << 1 (e.g. in the baseline condition, γ was ca. 4.5×10^{-4}). Such conditions (γ << 1) are required for the slope method to be valid.[25]

The sticking coefficient was back-extracted with the Arts et al.[30] slope method derived from the Yanguas-Gil and Elam model[20] as follows:

$$c = 13.9 \left(\left| \frac{d\theta}{d\tilde{x}} \right|_{\theta=1/2} \right)^2, \tag{29}$$

where θ (-) is the surface coverage and $\tilde{x}$ (-) is the dimensionless distance. In this work, the surface coverage θ was extracted from a Type 1 normalised thickness profile expressed as normalised thickness $s/(N\ gpc_{\mathrm{sat}})$ against dimensionless distance $\tilde{x}$. To back-extract the sticking coefficient the total number of discretisation points was selected so that the difference between the two discretisation points chosen in the *y*-axis was below 1% of the whole range.

[**] Note that Eq. 4 of Cremers et al.[4] for calculating the collision cross section contains an error: instead of taking the sum of squares ($r_i^2 + r_j^2$),[4] one should take the square of the sum $(r_i + r_j)^2$, where r_i (m) is the radius of molecule *i*. For the correct equation, see e.g. Eq. 24.3b Atkins and De Paula.[50]

4. Results and discussion

4.1. ALD in microchannels: general trends with the baseline process

Trends in the evolution of conformality in microchannels were initially investigated by defining a baseline process with parameters inspired by the experimental TMA-water process.[18,35,36,41] For these simulations, the microchannel height *H* was chosen to be 500 nm, as typically used in microscopic PillarHall™ LHAR structures.[18,30,36,42,43] The temperature was chosen to be 250 °C, which is in the typical temperature range of the TMA-water process.[31] The partial pressure of Reactant A and the inert gas were chosen as 100 Pa and 500 Pa, respectively, and the Reactant A pulse length was chosen as 0.1 s; these conditions are similar to earlier reported experimental conditions.[36,44] The adsorption density of the surface was set to 4 nm^{-2}, which is in the range observed for the TMA-water process[31,45,46] and in the range typical for ALD.[38] The molar mass of Reactant A was set to an arbitrary value of 100 $g\,mol^{-1}$, while that of the purge gas was typical for nitrogen (28 $g\,mol^{-1}$). The diameters of Reactant A and the inert gas were 600 and 374 pm, respectively, as in the TMA-water simulation.[18,36] The choice of H = 500 nm, combined with the pressure range used, resulted in the Knudsen number *Kn* for the baseline conditions being 7.6, which is in the transition flow regime ($0.1 \leq Kn \leq 10$).[24] The varied parameters are presented in Table 1.

Table 1. Process conditions selected for illustrating the effect of varied process conditions on the thickness profile in wide microchannels.* The baseline values are presented in **bold** font.

Parameter	Varied values	Effective *Kn*
p_{A0} (Pa)	50, **100**, 200, 400, 800	8.2, 7.6, 6.5, 5.0, 3.5
t_1 (s)	0.05, **0.1**, 0.2, 0.4, 0.8	7.6
M_A (kg mol^{-1})	0.0250, 0.050, **0.100**, 0.200, 0.400	10.7, 9.2, 7.6, 5.9, 4.5
ρ (kg m^{-3})	2500, 3000, **3500**, 4000, 4500	7.6
q (nm^{-2})	0.5, 1, 2, **4**, 8	7.6
P_d (s^{-1})	**0.01**, 0.1, 1, 10, 100	7.6
c (-)	0.0001, 0.001, **0.01**, 0.1, 1	7.6
T (°C)	50, 150, **250**, 350, 450	4.7, 6.1, 7.6, 9.0, 10.4
p_I (Pa)	0, 250, **500**, 750, 1000	45.2, 12.9, 7.6, 5.3, 4.1
H (µm)	0.1, 0.2, **0.5**, 1, 2, 2.5, 4	37.8, 18.9, 7.6, 3.8, 1.9, 1.5, 0.9
N (-)	5, 10, 20, 50, 100, **250**, 500	7.6

* Other baseline parameters used: W = 10 mm, d_A = 600 pm, d_I = 374 pm, M_I = 0.0280 kg mol^{-1}, b_{film} = 1, b_A = 1, and M = 0.050 kg mol^{-1}.

The thickness profiles simulated with varied parameters are shown in Figure 4(a)–(i). Panels (a) and (b), respectively, show that an increase in the partial pressure of Reactant A, p_A, and the pulse time of Reactant A, t_1, both significantly increase the penetration depth of the film. This result is as expected: the product of p_A and t_1 is the dose (Pa s) that defines the penetration depth at free molecular flow conditions (half-thickness penetration depth $\propto \sqrt{p_A t_1}$).[20,25,30] Panel (c) shows the effect of varying the molar mass of Reactant A, M_A. The penetration depth of the film is higher when the molecules are lighter. This is consistent with the fact that the diffusion of light molecules is faster than that of heavy

molecules (Eq. 4 and 7). Panel (d) illustrates the effect of varying the mass density of the grown M_yZ_x material, ρ. The lower the density, the higher the grown thickness (note that the penetration depth is not affected). With a lower density, one unit of M_yZ_x takes up a larger space, so a constant adsorption density q leads to a larger film volume and therefore a larger thickness (Eq. 12). (Note: the thickness-based GPC is not constant in such case.[3]) Panel (e) illustrates the effect of the adsorption density, q (i.e. GPC expressed as areal number density) on the thickness profile. With other parameters constant, the adsorption density has a strong influence on the growth. This is not surprising, since gpc_{sat} is the core parameter describing an ALD process.[1–3,28,31] The higher the gpc_{sat}, the higher the film thickness in the saturated region but the lower the penetration depth. This observation is consistent with and explains recent experimental findings where a higher gpc_{sat} resulted in a lower penetration depth.[36,41,47] Panel (f) shows how varying the desorption probability, P_d, affects the simulation (the Ylilammi et al.[18] model allows reversible reactions). High values of desorption probability affect the shape of the thickness profile especially in Region II, before the Region III of fast decrease (for regions, see Figure 1). Panel (g) illustrates the effect of varying the sticking coefficient of Reactant A, c. The sticking coefficient strongly affects the shape of the resulting thickness profile, as already known from earlier simulations.[12,29,30] Varying the process temperature T and the inert gas pressure p_I has a minor effect on the penetration depth, as seen from panels (h) and (i), respectively.

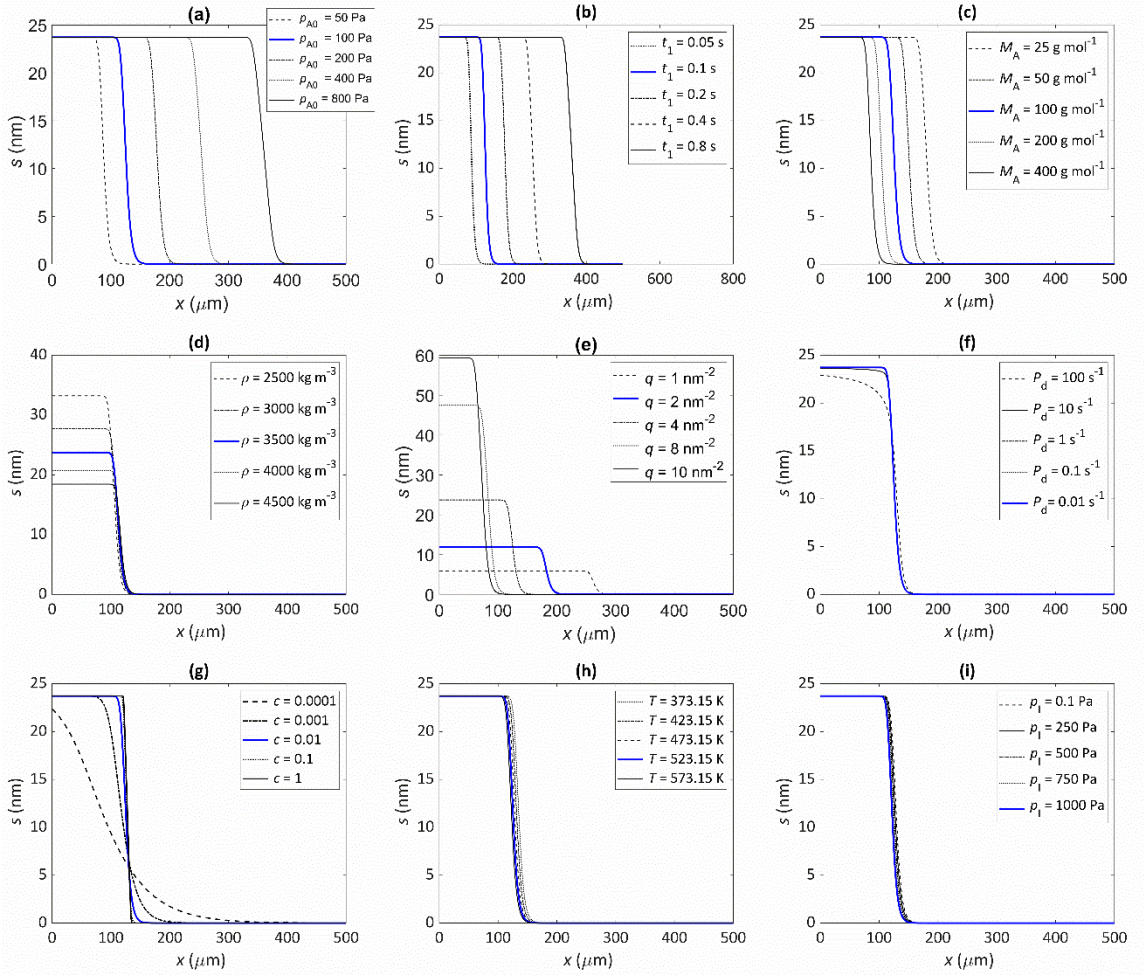

Figure 4. Illustration of the effect of varying individual parameters on the thickness profile in microchannels, simulated with the Ylilammi et al. model[18] re-implemented in this work. The parameter values used in the simulation are presented in Table 1. Simulations with the baseline values are shown as a solid blue line. The effect of the (a) initial partial pressure of the Reactant A, p_{A0}, (b) pulse length of Reactant A, t_1, (c) molecular mass of Reactant A, M_A, (d) film density, ρ, (e) adsorption density, q (i.e. GPC expressed as areal number density), (f) desorption probability, P_d, (g) (lumped) sticking coefficient, c, (h) ALD process temperature, T, and (i) inert gas pressure, p_I.

Earlier works have shown the importance of the sticking coefficient,[11,12,29] as well as the components defining the reactant dose [18,22,25] – i.e., reaction time and reactant

pressure – on the characteristics of the thickness profile. Simulations made in this work for a typical baseline process resembling the archetypical TMA-water ALD process demonstrated that the process parameters such as the molar mass of the reactant, the adsorption density (derived from the GPC), and the mass density of the film also influence the detailed features of the thickness profile.

4.2. Effect of filling of the microchannel on the simulated thickness profile

When a film grows into a microchannel, in each ALD cycle, the channel gets narrower from both sides by twice the value of the GPC (Eq. 24). The film thickness that completely fills the microchannel is thus half of the microchannel height *H*. Although an experimental ALD thickness profile can be measured after any number of cycles, the expected shape will depend on the number of ALD cycles, as shown in ref. 36.

How much can a microchannel be filled so that a "fingerprint" ALD thickness profile can be measured, whose shape and characteristics are not yet affected by the already grown film? From such fingerprint thickness profile, it is possible to extract the sticking coefficient with the simple slope method.[30] Earlier, a preferable filling of less than 10% was proposed.[36] Here, the effect of the channel filling on the resulting thickness profile was simulated, using the same baseline conditions as in the previous section (Table 1), and varying either the microchannel height *H* or the number of cycles *N*.

The results of the simulation series illustrating the effect of channel filling are shown in Figure 5. In the thickness profiles of panels (a) and (b), the expected features are observed: with a larger microchannel height, the penetration depth increases, and with an increasing number of cycles, the film thickness increases. The scaled thickness profiles of panels (c) and (d) reveal finer trends. With a constant film thickness and varied microchannel

height (c), the half-thickness penetration depth $\tilde{x}_{50\%}$ (-) first increases with increasing microchannel height, and then starts to decrease [panel (e)]. With a constant microchannel height and a varying film thickness of panel (d), the scaled thickness profiles simulated for the smallest cycle numbers (5 to 20) approximately overlap, but already for channel filling of a few percent, the penetration depth starts to decrease with channel filling [panel (e)]. Numerical information regarding the half-thickness penetration depth $\tilde{x}_{50\%}$ and the slope at this point is presented in Table S1.

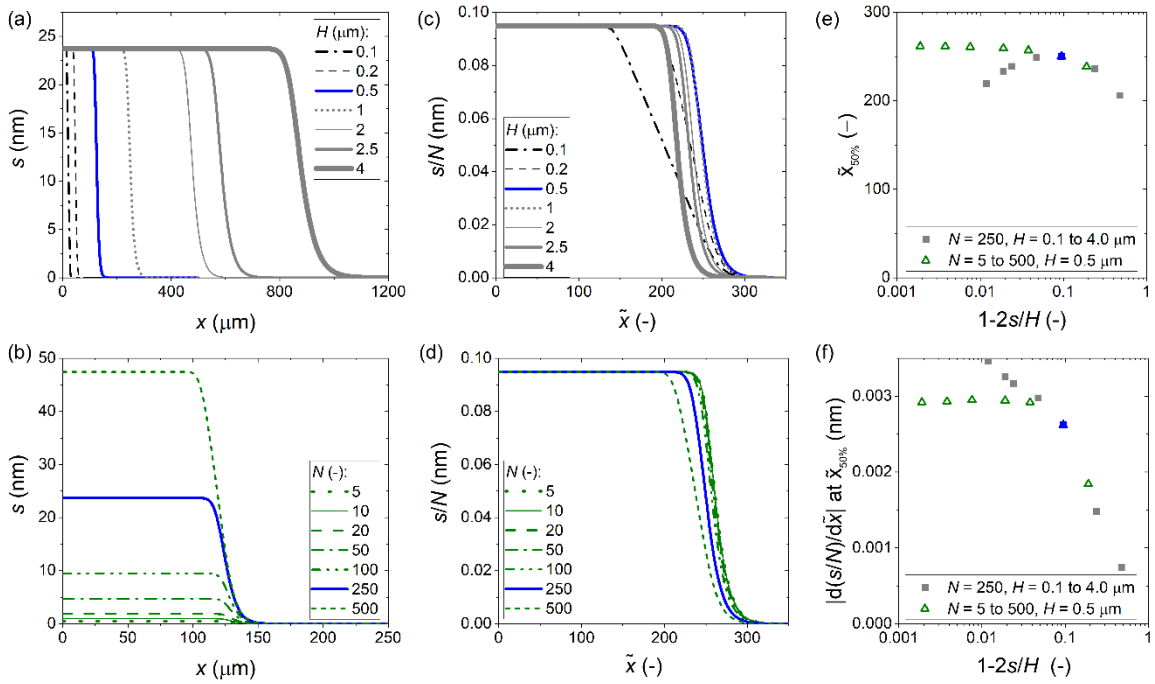

Figure 5. Illustration of the channel filling effect on the ALD thickness profile in wide microchannels. The parameters used in the simulations are given in Table 1. Baseline simulation results are marked in blue. (a) Thickness profiles simulated with a constant number of cycles of 250 and a varied channel height. (b) Thickness profiles simulated with a constant channel height of 500 nm and a varied number of cycles. (c) The scaled thickness profile from the data of panel (a). (d) The scaled thickness profile from the data of panel (b). (e) The half-thickness penetration depth of the scaled thickness profile as a function of the

channel filling fraction, for the data presented in panels (c) and (d). (f) The slope at half-thickness penetration depth as a function of the channel filling fraction (1–2*s*/*H*), from the data presented in panels (a/c) and (b/d).

The slope at half-thickness penetration depth is shown for both simulation series in Figure 5(f). For the series where the number of cycles was varied, the slope settles to a constant value (ca. −0.0029) for the smallest amounts of channel filling, as expected. The case where the channel height was varied, shows a different trend: with decreasing channel filling, after a knee, the absolute value of the slope increases again. Table S1 shows the Knudsen number *Kn* calculated in each case. The knee point occurs at *Kn* = 8 which is in the transition flow regime.[24] Because of the increasing channel height, the Knudsen number decreases with decreasing channel filling (see Figure S5). The reason for the somewhat unexpected trend of the increasing slope with increasing channel height (and decreasing channel filling) was the transition from free molecular flow towards transition flow (*Kn* < 10), where gas-phase collisions make the diffusion coefficient smaller.

From the simulations made to explore the effect of channel filling, the following can be concluded. (i) To be in the region where the thickness profile is independent of the number of cycles, the channel filling should not exceed a few percent. (ii) The flow regime affects the thickness profile, including the numerical characteristics of the half-thickness penetration depth and the slope at half-thickness penetration depth. To measure a fingerprint thickness profile for an ALD process, the flow condition must be free molecular flow (*Kn* >> 1). To check whether such is the case, the mean free path of the molecules should be calculated (Eq. 26) and compared to the limiting dimension of the feature (Eq. 25).

4.3. Comparison of thickness profile trends at free molecular flow and transition flow regimes

The simulations in the previous sections revealed that (i) the thickness profile characteristics depend on the flow regime and (ii) the thickness of the grown film affects the characteristics of the thickness profile already from a filling of a few percent.

To compare the trends of the ALD thickness profile in different flow regimes in a well-defined way, we varied individual process parameters to make ALD thickness profiles in free molecular flow ($Kn >> 1$) and transition flow ($Kn \approx 1$) conditions.[24,26,27] A comparison was made with a single cycle, so that the channel filling does not influence the trends of the thickness profile. Both the scaled thickness profile and the Type 1 normalized thickness profile were used as a basis for comparison. The scaled thickness profile is the most informative thickness profile for an ALD process, and the Type 1 normalized thickness profile is the basis of the slope method.[30] The thickness profiles are presented in Figures S6 to S9. For each case, the trends in the half-thickness penetration depth $\tilde{x}_{50\%}\ (-)$ and the absolute value of the slope at $\tilde{x}_{50\%}$ were analysed. The numerical values are shown in Figures S10 to S15.

The qualitative thickness profile trends in the free molecular flow and transition flow regimes are summarised in Table 2. In free molecular flow, the half-thickness penetration depth and the absolute value of the slope remained constant with varying channel heights, as expected. In transition flow, the penetration depth decreased, and the absolute value of the slope increased with increasing channel heights, most likely resulting from gas-phase collisions. An increase of the reactant partial pressure and pulse time highly increased the penetration depth in both free molecular flow and transition flow, as expected. The desorption probability did not affect the penetration depth and the absolute value of the

slope in either flow regime. The penetration depth decreased slightly with the increasing process temperature in both flow regimes.

Some process parameters affected the trends of the thickness profile differently in different flow regimes. The molar mass of Reactant A did not affect the absolute value of the slope in free molecular flow while the absolute value of the slope slightly increased with increasing molar mass in the transition flow. The inert gas influenced thickness profile differently in free molecular flow and transition flow. The inert gas parameters did not affect the penetration depth or the slope in the free molecular flow regime, as expected. In the transition flow regime, the half-thickness penetration depth slightly decreased with increasing pressure and decreasing molar mass of the inert gas. The absolute value of the slope slightly increased with the increasing pressure and decreasing molar mass of inert gas. The absolute value of the slope in the transition flow regime slightly increased with increasing reactant size, while the reactant size did not affect thickness profile in the free molecular flow regime.

In general, the scaled thickness profile showed the same trends as the Type 1 normalized thickness profile. However, there were two exceptions. With increasing adsorption density q, the absolute value of the slope of the scaled thickness profile markedly increased, while that of the Type 1 normalized thickness profile remained constant. With increasing density of grown film ρ, the absolute value of the slope of the scaled thickness profile slightly decreased, while that of the Type 1 normalized thickness profile remained constant.

Table 2. Summary of the qualitative effects of varying specific parameters on the thickness profile, characterised by the half-thickness penetration depth and the slope at half-thickness

510 penetration depth. The trends are reported separately for different diffusion regimes: free
511 molecular flow (*Kn* >> 1) and transition flow (*Kn* ≈ 1). Indicators: ↑ increases slightly, ↑↑
512 increases markedly, and ↑↑↑ increases strongly, - no change, ↓ decreases slightly, ↓↓
513 decreases markedly with increasing parameter values.[a)]

Simulation parameter (increases)	*Kn* >> 1			*Kn* ≈ 1		
	$\tilde{x}_{50\%}$	$\left\lvert\frac{\mathrm{d}\left(\frac{s}{N}\right)}{\mathrm{d}\tilde{x}}\right\rvert_{\tilde{x}_{50\%}}$	$\left\lvert\frac{\mathrm{d}\theta}{\mathrm{d}\tilde{x}}\right\rvert_{\theta=1/2}$	$\tilde{x}_{50\%}$	$\left\lvert\frac{\mathrm{d}\left(\frac{s}{N}\right)}{\mathrm{d}\tilde{x}}\right\rvert_{\tilde{x}_{50\%}}$	$\left\lvert\frac{\mathrm{d}\theta}{\mathrm{d}\tilde{x}}\right\rvert_{\theta=1/2}$
	(-)	(nm)	(-)	(-)	(nm)	(-)
Channel height (*H*)	-	-	-	↓	↑	↑
Initial partial pressure of the ALD Reactant A (p_{A0})	↑↑	-	-	↑↑	-	-
Reactant pulse time (t_1)	↑↑↑	-	-	↑↑↑	-	-
Sticking coefficient(*c*)	↑	↑↑↑	↑↑↑	↑	↑↑↑	↑↑↑
Desorption probability (P_d)	-	-	-	-	-	-
Adsorption density (*q*)	↓↓↓	↑↑	-	↓↓↓	↑↑	-
Temperature (*T*)	↓	-	-	↓	-	-
Total pressure (p)[b)]	-	-	-	↓	↑	↑
Fraction of reactant pressure of total pressure (p_{A0}/p)[c)]	↑↑	-	-	↑↑	-	-

Molecular mass of the ALD reactant (M_A)	↓	-	-	↓	↑	↑
Molecular mass of the carrier gas (M_I)	-	-	-	↑	↓	↓
Size of the reactant molecule (d_A)	-	-	-	-	↑	↑
Density of the grown material (ρ)	-	↓	-	-	↓	-

a) The parameter values used for the centre point in the free molecular flow regime were: W = 0.01 m, $H = 5 \times 10^{-8}$ m, N = 1, t_1 = 0.1 s, p_{A0} = 50 Pa, M_A = 0.1 kg mol^{-1}, $d_A = 6.0 \times 10^{-10}$ m, M_I = 0.028 kg mol^{-1}, $d_I = 4.0 \times 10^{-10}$ m, p_I = 250 Pa, $q = 4 \times 10^{18}$ m^{-2}, ρ = 3500 kg m^{-3}, M = 0.050 kg mol^{-1}, P_d = 0.01 s^{-1}, and c = 0.01. The parameter values used for the centre point in transition flow regimes were: W = 0.01 m, $H = 5 \times 10^{-7}$ m, N = 1, t_1 = 0.1 s, p_{A0} = 500 Pa, M_A = 0.1 kg mol^{-1}, $d_A = 6.0 \times 10^{-10}$ m, M_I = 0.028 kg mol^{-1}, $d_I = 4.0 \times 10^{-10}$ m, p_I = 2500 Pa, $q = 4 \times 10^{18}$ m^{-2}, ρ = 3500 kg m^{-3}, M = 0.050 kg mol^{-1}, P_d = 0.01 s^{-1}, and c = 0.01.

b) The total pressure p was increased by increasing the partial pressure of the inert gas p_I from 0.5 to 250 Pa with a constant reactant partial pressure p_{A0} of 100 Pa in free molecular flow and by increasing the partial pressure of the inert gas p_I from 62.5 to 1000 Pa with constant reactant partial pressure p_{A0} of 500 Pa in transition flow.

c) The initial partial pressure of Reactant A was varied from 1 to 100 Pa, with a constant partial pressure of the inert gas p_I of 250 Pa in free molecular flow. The initial partial pressure of Reactant A was varied from 100 to 1000 Pa, with a constant partial pressure of the inert gas p_I of 2500 Pa in transition flow.

4.4. Comparison of the simulations with different models

To compare the Ylilammi et al.[18] model (Model A) and the slope method[30] derived from the Yanguas-Gil and Elam[20] model (Model B), sticking coefficients were back-extracted with the slope method[25] (Eq. 29) from simulated thickness profiles obtained by Model A and Model B. Different scenarios with varying process temperatures, molar masses, and sticking coefficients were tested, with parameters defined so that the mass transport was always in the free molecular flow regime ($Kn \geq 100$), and the excess number γ was << 1,[33] as it is where the slope method[30] is valid. Figure 6 (a) shows that when $Kn \geq 100$, the effective diffusion coefficient D_{eff} becomes practically identical to the Knudsen diffusion coefficient D_{Kn}. Note that the comparison was made at conditions where the number of ALD cycles was one. If a larger number of cycles were used and part of the microchannel got filled by the growing film, the slope and penetration depth would have decreased. This channel filling would affect the extracted sticking coefficient and, thus, the comparison.

Figure 6 panels (b) to (d) show the sticking coefficients back-extracted by the slope method[30] compared to set values. Table 3 lists the parameter values used for simulations and the back-extracted sticking coefficients. Figure S16 shows Type 1 normalized thickness profiles used for the back extraction of (lumped) sticking coefficients. While the order of magnitude is the same, the back-extracted sticking coefficients are systematically ca. 25% higher than the set values (see Table 3). Therefore, it seems that the slope method[30] can be used to back-extract sticking coefficients from thickness profiles simulated with the current implementation of the Ylilammi et al.[18] model by simply applying a correction factor.

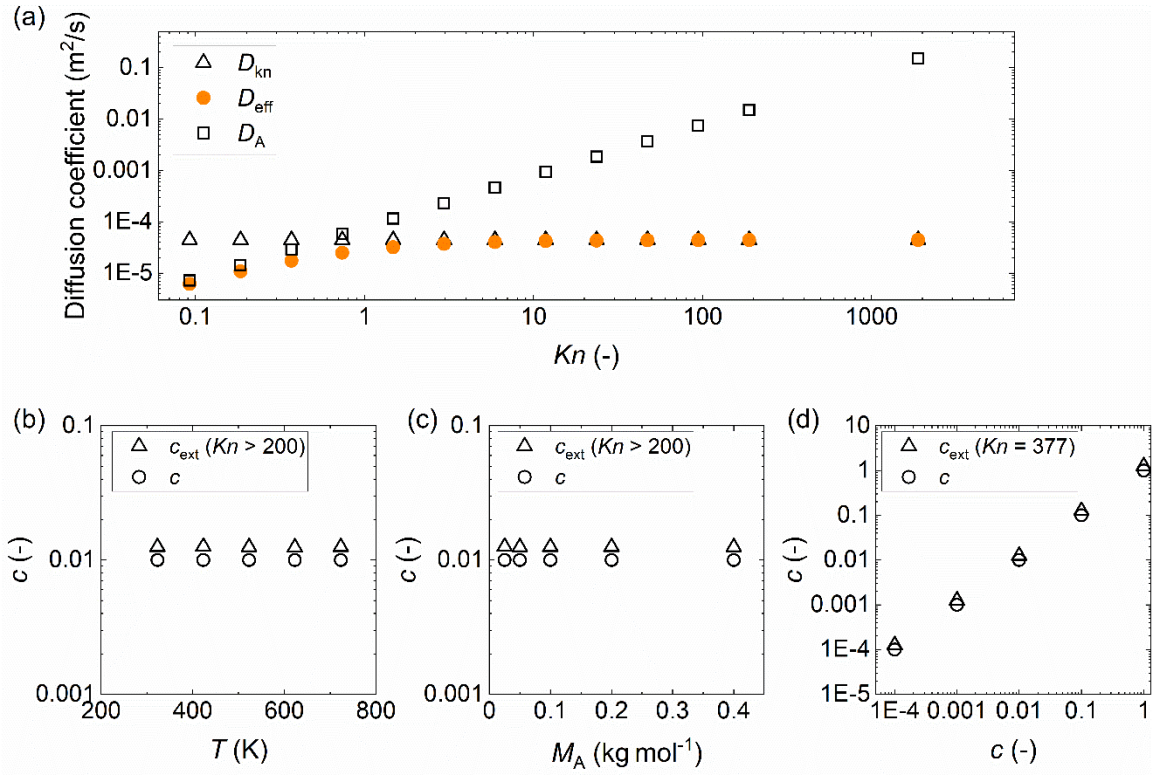

552

553 Figure 6. (a) Diffusion coefficients (Eqs. 2, 4, and 7) against the Knudsen number (*Kn*).
554 Knudsen numbers were varied by varying p_{A0} from 1 to 20480 Pa (the p_{A0} to p_I ratio was 1 to
555 5). A comparison of the sticking coefficient values back-extracted using the slope method [30]
556 (marked with open triangles) with the set values (marked with open circles) used for
557 simulation, implementing the Ylilammi et al. model[18] with different (b) ALD process
558 temperatures, *T*, (c) molar masses of Reactant A, M_A, and (d) sticking coefficients. The
559 parameter values used, if not otherwise stated: *W* = 10 mm, *H* = 100 nm, *N* = 1, T = 523.15 K,
560 t_1 = 2 s, p_{A0} = 10 Pa, M_A = 0.1 kg mol^{-1}, d_A = 6.0 × 10^{-10} m, M_I = 0.028 *kg* mol^{-1}, d_I = 3.74 × 10^{-10}
561 m, p_I = 50 Pa, *q* = 4 × 10^{-18} m^{-2}, *ρ* = 3500 kg m^{-3}, *M* = 0.050 kg mol^{-1}, P_d = 10^{-5} s^{-1}, and *c* = 0.01.

562 Table 3. Sticking coefficient values back-extracted (c_{ext}) by the slope method [30] against the ones (c) used in simulations implementing the

563 Ylilammi et al. model [18] with varying process temperatures, molar masses of Reactant A, and sticking coefficients*

Series	T (K)	M_A (kg mol^{-1})	c (-)	Kn (-)	$\left\|\frac{d\theta}{d\tilde{x}}\right\|_{\theta=1/2}$ (-)	c_{ext} (-)	c_{ext} /c (-)
ALD process temperature	**323.15**	0.1	0.01	233	0.0300	0.0125	1.25
	423.15	0.1	0.01	305	0.0301	0.0126	1.26
	523.15	0.1	0.01	378	0.0300	0.0125	1.25
	623.15	0.1	0.01	450	0.0300	0.0125	1.25
	723.15	0.1	0.01	522	0.0300	0.0125	1.25
Molar mass of Reactant A	523.15	**0.025**	0.01	537	0.0301	0.0126	1.26
	523.15	**0.05**	0.01	462	0.0300	0.0125	1.25
	523.15	**0.1**	0.01	378	0.0300	0.0125	1.25
	523.15	**0.2**	0.01	295	0.0300	0.0125	1.25
	523.15	**0.4**	0.01	223	0.0300	0.0125	1.25
	523.15	0.1	**0.0001**	378	0.0030	0.000126	1.26

Sticking coefficient	523.15	0.1	**0.001**	378	0.0095	0.00125	1.25
	523.15	0.1	**0.01**	378	0.0300	0.0125	1.25
	523.15	0.1	**0.1**	378	0.0951	0.126	1.26
	523.15	0.1	**1**	378	0.3004	1.25	1.25

564 * Parameters used, if not otherwise stated: W = 0.01 m, H = 10^{-7} m, T = 523.15 K, N = 1, t_1 = 2 s, p_{A0} = 10 Pa, M_A = 0.1 kg mol^{-1}, d_A = 6.0 ×
565 10^{-10} m, M_I = 0.028 kg mol^{-1}, d_I = 3.74 × 10^{-10} m, p_I = 50 Pa, q = 4 × 10^{-18} m^{-2}, ρ = 3500 kg m^{-3}, M = 0.050 kg mol^{-1}, P_d = 10^{-5} s^{-1}, and c =
566 0.01. To satisfy the criteria of a difference between the two discretisation points in the y-axis below 1% of the whole range, 5000
567 discretisation points were used in the simulations with varied molar mass of Reactant A and process temperature while in the
568 simulation with varied sticking coefficient 30000 discretization points were used.
569

To analyse possible sources of differences in the sticking coefficient values, we compared the partial pressure of Reactant A along the microchannels simulated with the Ylilammi et al.[18] model (Model A) and the Yanguas-Gil and Elam[20] model (Model B); Model B forms the basis of the slope method.[30] Figure 7 shows the surface coverage and partial pressure simulated with the above two models against the dimensionless distance. Figure 7 (b) shows observable differences in partial pressures and coverage profiles especially in Region III of the thickness profile [regions are shown in Figure 1 (b)], which is the adsorption front where the thickness rapidly decreases.[36] A difference is expected, since the Ylilammi et al.[18] model introduced a simplified analytical approximation to the partial pressure (Eqs. 8 and 9) (Figure S1). We conclude that the more rapid drop of pressure p_A at the adsorption front simulated by Model A caused a higher absolute slope value extracted at half-thickness penetration depth, and thus a slightly higher back-extracted sticking coefficient compared to that of Model B.

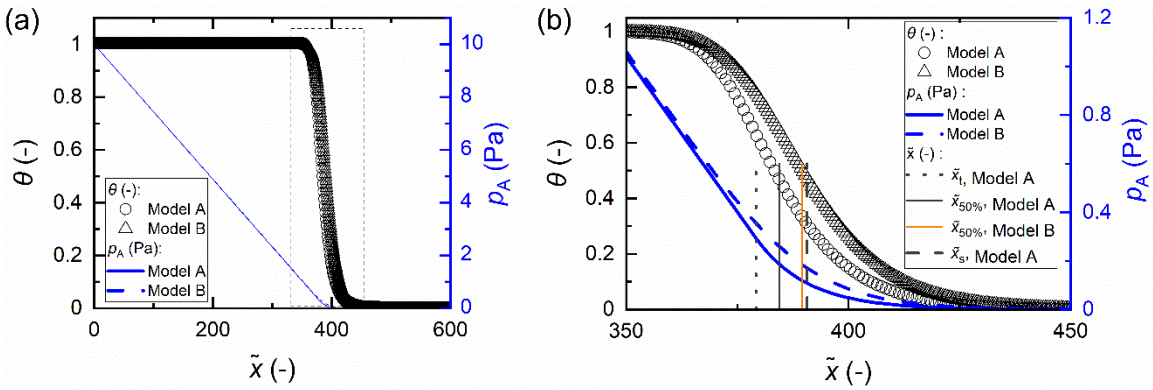

Figure 7. (a) Surface coverage θ and partial pressure of Reactant A p_A within the dimensionless distance $\tilde{x}$ simulated by model A (ref. 18) and model B (ref. 20). (b) Details of the area marked with a square in panel (a). Parameter values used: c = 0.01, t_1 = 2 s, T = 523.15 K, p_{A0} = 10 Pa, N = 1, M_A = 0.1 kg mol^{-1}, d_A = 6.0 × 10^{-10} m, p_I = 50 Pa, M_I = 0.028 kg mol^{-1}, d_I = 3.74 × 10^{-10} m, ρ = 3500 kg m^{-3}, M = 0.050 kg mol^{-1}, P_d = 10^{-5} s^{-1}, q = 4 × 10^{-18} m^{-2}, H = 5 × 10^{-7} m, and W = 0.01 m.

5. Conclusion and outlook

This work re-implemented the Ylilammi et al.[18] diffusion-reaction model for ALD conformality analysis through thickness profile simulation and used that model to explore trends in the thickness profile inside wide microchannels at different diffusion regimes encountered in reality.

A series of simulations were made to explore the effect on thickness profile characteristics at free molecular flow and transition flow conditions of kinetic and process parameters, such as temperature, (lumped) sticking coefficient, molar mass of the ALD reactant, the reactant's exposure time and pressure, total pressure, density of the grown material, and GPC of the ALD process. Increasing the molar mass and the GPC, for example, resulted in a decreasing penetration depth into the LHAR channel. Trends with parameter changed depending on the flow regime. To obtain an ALD measurable or a "fingerprint" characteristic for a specific ALD process the following conditions should be met: (i) free molecular flow should be the governing mass transport regime, (ii) the channel filling should remain below 5%, and (iii) the scaled thickness profile should be presented, with the dimensionless distance on the horizontal axis and the thickness divided by cycles on the vertical axis. From such fingerprint thickness profile, the characteristic GPC is evident, and the kinetic information can be extracted by various means.

The simulations were compared with the recent slope method by back-extracting the sticking coefficient from the ALD thickness profiles at free molecular flow conditions. The slope method gave systematically somewhat higher sticking coefficient values than input values. The difference is most likely related to how, to speed up simulations, the

611 partial pressure of Reactant A inside the channel is analytically approximated in the re-
612 implemented model.

613 For reactor modelling, kinetic information of real ALD processes is needed.
614 Recent advances have made it possible to measure experimental thickness profiles, which
615 contain the necessary kinetic information, without the need of time-consuming post-
616 preparation of HAR samples. Several theoretical models have been developed to extract
617 (lumped) sticking coefficient parameters from such experimental data. This work has shown
618 that (i) to obtain experimental data for kinetic experiments, detailed knowledge of the
619 experimental conditions, especially pressure, is important, to choose a suitable model for the
620 parameter extraction (most models are based on free molecular flow assumption).
621 Furthermore, (ii) there are differences between the models. The same data fitted with
622 different models may give different results for the extracted fundamental kinetic growth
623 parameters, as the details of the model implementation may affect the results.

624 For speedy development of the fundamental understanding of ALD processes,
625 and to compare models with each other and with data, it would be advantageous if the
626 scientific ALD community could publish experimental thickness profiles as Open Data and
627 models as Open Code. First such initiatives have already been made: an Open Data
628 community has been initiated in Zenodo.org,[48] and the first ALD simulation code has been
629 published in Github.[49] The simulation codes of this work are to be published accordingly.

630 Conflict of interest

631 There are no conflicts of interest to declare.

Acknowledgements

The authors thank Dr. Angel Yanguas-Gil, Prof. J. Ruud van Ommen, Prof. Ville Alopaeus, Prof. Ville Vuorinen, Gizem Ersavas Isitman and Jänis Järvilehto for useful discussions on ALD modelling. Part of the results presented of this work were presented at the international ALD conferences, organised virtually by the American Vacuum Society (AVS) in 2020 and 2021. The MATLAB simulation codes created in this work will be made openly available. A community for open data related to the experimental and simulated ALD thickness profiles is available at https://zenodo.org/communities/ald-saturation-profile-open-data/.

Funding sources

The work was financially supported by the Academy of Finland (COOLCAT consortium, decision no. 329978 and ALDI consortium, decision no. 331082) and by Prof. Puurunen's starting grant at Aalto University.

List of symbols

b	Number of metal atoms in a reactant molecule in the Ylilammi et al.[18] model (-)
c	Sticking coefficient (-)
c_{ext}	Sticking coefficient back-extracted with the slope method[30] (-)
D	Apparent longitudinal diffusion coefficient in the Ylilammi et al.[18] model (m^2 s^{-1})
D_A	Gas-phase diffusion coefficient of Reactant A (m^2 s^{-1})
D_{eff}	Effective diffusion coefficient (m^2 s^{-1})

D_{Kn}	Knudsen diffusion coefficient ($m^2\,s^{-1}$)
d_A	Hard-sphere diameter of molecule A (m)
d_I	Hard-sphere diameter of the inert gas molecule (m)
f_{ads}	Adsorption rate ($m^{-2}\,s^{-1}$)
f_{des}	Desorption rate ($m^{-2}\,s^{-1}$)
g	Net adsorption rate ($m^{-2}\,s^{-1}$)
gpc_{sat}	Saturation growth per cycle, thickness-based, in the Ylilammi et al.[18] model (m)
h	Hydraulic diameter of the channel (m)
H	Height of the channel (m)
K	Adsorption equilibrium constant in the Ylilammi et al.[18] model (Pa^{-1})
Kn	Knudsen number (-)
k_B	Boltzmann constant ($m^2\,kg\,s^{-2}\,K^{-1}$)
L	Length of the channel (m)
M	Molar mass of the deposited film material ($kg\,mol^{-1}$)
M_A	Molar mass of Reactant A ($kg\,mol^{-1}$)
M_I	Molar mass of the inert gas I ($kg\,mol^{-1}$) (M_B in Ylilammi et al.[18])
N	Number of ALD cycles
n_A	Particle concentration of Reactant A (m^{-3})
N_0	Avogadro's constant (mol^{-1})
p	Total pressure ($p_{A0} + p_I$) (Pa)
p_A	Partial pressure of Reactant A (Pa)
p_{A0}	Initial partial pressure of Reactant A (Pa)

p_I	Partial pressure of the inert gas I (Pa)
p_At	Partial pressure of Reactant A at x_t (Pa)
P_d	Desorption probability in unit time in the Ylilammi et al.[18] model (s^{-1})
q	Adsorption density of metal M atoms in the growth of film of the M_yZ_x material (m^{-2}) (i.e. GPC expressed as areal number density)
Q	Collision rate with surface at unit pressure in the Ylilammi et al.[18] model ($m^{-2}\ s^{-1}\ Pa^{-1}$)
r_i	Hard-sphere radius of molecule *i* (m)
R	Gas constant (8.3144626 $J\ K^{-1}\ mol^{-1}$)
s	Film thickness in the Ylilammi et al.[18] model (m)
S	Surface area of the microchannel (m^2)
t	Time (s)
t_1	Length of the Reactant A pulse (as Step 1 of a typical ALD cycle[3]) (s)
T	Temperature (K)
v	Velocity of gas front in the Ylilammi et al.[18] model ($m\ s^{-1}$)
V	Volume of the microchannel (m^3)
$\bar{v}_\mathrm{A}$	Average speed of molecules A ($m\ s^{-1}$)
W	Width of the channel (m)
x	Distance from the channel entrance (m)
$x_{50\%}$	Half-thickness penetration depth (m) (expressed as x_p in Ylilammi et al.[18])
$\tilde{x}$	Dimensionless distance into the channel, x/H (-)
$\tilde{x}_{50\%}$	Half-thickness penetration depth (-)

x_s	Distance where the extrapolated linear part of the reactant pressure is zero in the Ylilammi et al.[18] model (m)
x_t	Distance of the linear part of the reactant pressure distribution in the Ylilammi et al.[18] model (m)
z_A	Collision frequency of Reactant A with other gas molecules in a gas mixture of Reactant A + inert gas I (s^{-1})
θ	Surface coverage (-), $0 \leq \theta \leq 1$
ρ	Mass density of the deposited film ($kg\,m^{-3}$)
λ	Mean free path (m)
$\sigma_{i,j}$	Collision cross section between the molecules *i* and *j* (m^2)
γ	Excess number in the Yanguas-Gil and Elam[20] model (-)

References

1 T. Suntola, Atomic layer epitaxy, *Materials Science Reports*, 1989, **4**, 261–312.

2 M. G. Steven, Atomic Layer Deposition: An Overview, *Chemical Reviews*, 2010, **110**, 111–131.

3 J. R. van Ommen, A. Goulas and R. L. Puurunen, Atomic layer deposition, *Kirk-Othmer Encyclopedia of Chemical Technology*, John Wiley & Sons, Inc, 2021.

4 V. Cremers, R. L. Puurunen and J. Dendooven, Conformality in atomic layer deposition: current status overview of analysis and modelling, *Applied Physics Reviews*, 2019, **6**, 021302.

5 N. Cheimarios, G. Kokkoris and A. G. Boudouvis, Multiscale Modeling in Chemical Vapor Deposition Processes: Models and Methodologies, *Archives of Computational Methods in Engineering*, 2021, **28**, 637–672.

6 A. Yanguas-Gil and J. W. Elam, A Markov chain approach to simulate atomic layer deposition chemistry and transport inside nanostructured substrates, *Theoretical Chemistry Accounts*, 2014, **133**, 1465.

7 R. A. Adomaitis, A ballistic transport and surface reaction model for simulating atomic layer deposition processes in high-aspect-ratio nanopores, *Chemical Vapor Deposition*, 2011, **17**, 353–365.

8 J.-Y. Kim, J.-H. Kim, J.-H. Ahn, P.-K. Park and S.-W. Kang, Applicability of Step-Coverage Modeling to TiO2 Thin Films in Atomic Layer Deposition, *Journal of The Electrochemical Society*, 2007, **154**, H1008.

9 M. K. Gobbert, V. Prasad and T. S. Cale, Predictive modeling of atomic layer deposition on the feature scale, *Thin Solid Films*, 2002, **410**, 129–141.

10 J. W. Elam, D. Routkevitch, P. P. Mardilovich and M. G. Steven, Conformal coating on ultrahigh-aspect-ratio nanopores of anodic alumina by atomic layer deposition, *Chemistry of Materials*, 2003, **15**, 3507–3517.

11 M. C. Schwille, T. Schössler, J. Barth, M. Knaut, F. Schön, A. Höchst, M. Oettel and J. W. Bartha, Experimental and simulation approach for process optimization of atomic layer deposited thin films in high aspect ratio 3D structures, *Journal of Vacuum Science & Technology A: Vacuum, Surfaces, and Films*, 2016, **35**, 01B118.

12 M. Rose and J. W. Bartha, Method to determine the sticking coefficient of precursor molecules in atomic layer deposition, *Applied Surface Science*, 2009, **255**, 6620–6623.

13 V. Cremers, F. Geenen, C. Detavernier and J. Dendooven, Monte Carlo simulations of atomic layer deposition on 3D large surface area structures: Required precursor exposure for pillar- versus hole-type structures, *Journal of Vacuum Science & Technology A: Vacuum, Surfaces, and Films*, 2016, **35**, 01B115.

14 H. C. M. Knoops, E. Langereis, M. C. M. van de Sanden and W. M. M. Kessels, Conformality of Plasma-Assisted ALD: Physical Processes and Modeling, *Journal of The Electrochemical Society*, 2010, **157**, G241–G249.

15 J. Dendooven, D. Deduytsche, J. Musschoot, R. L. Vanmeirhaeghe and C. Detavernier, Conformality of Al2O3 and AlN Deposited by Plasma-Enhanced Atomic Layer Deposition, *Journal of The Electrochemical Society*, 2010, **157**, G111–G116.

16 H. Shimizu, K. Sakoda, T. Momose, M. Koshi and Y. Shimogaki, Hot-wire-assisted atomic layer deposition of a high quality cobalt film using cobaltocene: Elementary reaction analysis on NHx radical formation, *Journal of Vacuum Science & Technology A*, 2012, **30**, 01A144.

17 P. Poodt, A. Mameli, J. Schulpen, W. M. M. (Erwin) Kessels and F. Roozeboom, Effect of reactor pressure on the conformal coating inside porous substrates by atomic layer deposition, *Journal of Vacuum Science & Technology A*, 2017, **35**, 021502.

18 M. Ylilammi, O. M. E. Ylivaara and R. L. Puurunen, Modeling growth kinetics of thin films made by atomic layer deposition in lateral high-aspect-ratio structures, *Journal of Applied Physics*, 2018, **123**, 205301.

19 H. Y. Lee, C. J. An, S. J. Piao, D. Y. Ahn, M. T. Kim and Y. S. Min, Shrinking core model for Knudsen diffusion-limited atomic layer deposition on a nanoporous monolith with an ultrahigh aspect ratio, *Journal of Physical Chemistry C*, 2010, **114**, 18601–18606.

20 A. Yanguas-Gil and J. W. Elam, Self-limited reaction-diffusion in nanostructured substrates: Surface coverage dynamics and analytic approximations to ALD saturation times, *Chemical Vapor Deposition*, 2012, **18**, 46–52.

21 A. J. Gayle, Z. J. Berquist, Y. Chen, A. J. Hill, J. Y. Hoffman, A. R. Bielinski, A. Lenert and N. P. Dasgupta, Tunable Atomic Layer Deposition into Ultra-High-Aspect-Ratio (>60000:1) Aerogel Monoliths Enabled by Transport Modeling, *Chemistry of Materials*, 2021, **33**, 5572–5583.

22 W. Z. Fang, Y. Q. Tang, C. Ban, Q. Kang, R. Qiao and W. Q. Tao, Atomic layer deposition in porous electrodes: A pore-scale modeling study, *Chemical Engineering Journal*, 2019, **378**, 122099.

23 H. van Bui, F. Grillo and J. R. van Ommen, Atomic and molecular layer deposition: off the beaten track, *Chemical Communications*, 2017, **53**, 45–71.

24 S. Roy, R. Raju, H. F. Chuang, B. A. Cruden and M. Meyyappan, Modeling gas flow through microchannels and nanopores, *Journal of Applied Physics*, 2003, **93**, 4870–4879.

25 R. G. Gordon, D. Hausmann, E. Kim and J. Shepard, A kinetic model for step coverage by atomic layer deposition in narrow holes or trenches, *Chemical Vapor Deposition*, 2003, **9**, 73–78.

26 A. Yanguas-Gil, *Growth and Transport in Nanostructured Materials: Reactive Transport in PVD, CVD, and ALD*, Springer, 2016.

27 Z. Li, K. Cao, X. Li and R. Chen, Computational fluid dynamics modeling of spatial atomic layer deposition on microgroove substrates, *International Journal of Heat and Mass Transfer*, 2021, **181**, 121854.

28 H. H. Sønsteby, A. Yanguas-Gil and J. W. Elam, Consistency and reproducibility in atomic layer deposition, *Journal of Vacuum Science & Technology A*, 2020, **38**, 020804.

29 J. Dendooven, D. Deduytsche, J. Musschoot, R. L. Vanmeirhaeghe and C. Detavernier, Modeling the Conformality of Atomic Layer Deposition: The Effect of Sticking Probability, *Journal of The Electrochemical Society*, 2009, **156**, P63–P67.

30 K. Arts, V. Vandalon, R. L. Puurunen, M. Utriainen, F. Gao, W. M. M. Kessels and H. C. M. Knoops, Sticking probabilities of H2O and Al(CH3)3 during atomic layer deposition of Al2O3 extracted from their impact on film conformality, *Journal of Vacuum Science & Technology A*, 2019, **37**, 030908.

31 R. L. Puurunen, Surface chemistry of atomic layer deposition: A case study for the trimethylaluminum/water process, *Journal of Applied Physics*, 2005, **97**, 121301.

32 J. Aarik and H. Siimon, Characterization of adsorption in flow type atomic layer epitaxy reactor, *Applied Surface Science*, 1994, **81**, 281–287.

33 A. Yanguas-Gil and J. W. Elam, Simple model for atomic layer deposition precursor reaction and transport in a viscous-flow tubular reactor, *Journal of Vacuum Science & Technology A*, 2012, **30**, 01A159.

34 PillarHall, http://www.pillarhall.com/, (accessed August 23, 2021).

35 F. Gao, S. Arpiainen and R. L. Puurunen, Microscopic silicon-based lateral high-aspect-ratio structures for thin film conformality analysis, *Journal of vacuum science & Technology A*, 2015, **33**, 010601.

36 J. Yim, O. M. E. Ylivaara, M. Ylilammi, V. Korpelainen, E. Haimi, E. Verkama, M. Utriainen and R. L. Puurunen, Saturation profile based conformality analysis for atomic layer deposition: Aluminum oxide in lateral high-aspect-ratio channels, *Physical Chemistry Chemical Physics*, 2020, **22**, 23107–23120.

37 E. Haimi, O. M. E. Ylivaara, J. Yim and R. L. Puurunen, Saturation profile measurement of atomic layer deposited film by X-ray microanalysis on lateral high-aspect-ratio structure, *Applied Surface Science Advances*, 2021, **5**, 100102.

38 T. Blomberg, (Invited) Unit Steps of an ALD Half-Cycle, *ECS Transactions*, 2013, **58**, 3–18.

39 pdepe, https://www.mathworks.com/help/matlab/ref/pdepe.html, (accessed August 23, 2021).

40 S. Chapman and T. G. Cowling, *The Mathematical Theory of Non-Uniform Gases: An Account of the Kinetic Theory of Viscosity: An Account of the Kinetic Theory of Viscosity, Thermal Conduction and Diffusion in Gases*, Cambridge University Press, 1970.

41 R. L. Puurunen and F. Gao, Influence of ALD temperature on thin film conformality: Investigation with microscopic lateral high-aspect-ratio structures, *14th International Baltic Conference on Atomic Layer Deposition (BALD), St. Petersburg (IEEE)*, 2016, 20–24.

42 K. Arts, J. H. Deijkers, T. Faraz, R. L. Puurunen, W. M. M. E. Kessels and H. C. M. Knoops, Evidence for low-energy ions influencing plasma-assisted atomic layer deposition of SiO2: Impact on the growth per cycle and wet etch rate, *Applied Physics Letters*, 2020, **117**, 031602.

43 K. Arts, M. Utriainen, R. L. Puurunen, W. M. M. E. Kessels and H. C. M. Knoops, Film Conformality and Extracted Recombination Probabilities of O Atoms during Plasma-assisted Atomic Layer Deposition of SiO2, TiO2, Al2O3, and HfO2, *The journal of Physical Chemistry C*, 2019, 1–11.

44 O. M. E. Ylivaara, L. Kilpi, X. Liu, S. Sintonen, S. Ali, M. Laitinen, J. Julin, E. Haimi, T. Sajavaara, H. Lipsanen, S.-P. Hannula, H. Ronkainen and R. L. Puurunen, Aluminum oxide/titanium dioxide nanolaminates grown by atomic layer deposition: Growth and mechanical properties, *Journal of Vacuum Science & Technology A: Vacuum, Surfaces, and Films*, 2017, **35**, 01B105.

45 R. L. Puurunen, Correlation between the growth-per-cycle and the surface hydroxyl group concentration in the atomic layer deposition of aluminum oxide from trimethylaluminum and water, *Applied Surface Science*, 2005, **245**, 6–10.

46 O. M. E. Ylivaara, X. Liu, L. Kilpi, J. Lyytinen, D. Schneider, M. Laitinen, J. Julin, S. Ali, S. Sintonen, M. Berdova, E. Haimi, T. Sajavaara, H. Ronkainen, H. Lipsanen, J. Koskinen, S.-P. Hannula and R. L. Puurunen, Aluminum oxide from trimethylaluminum and water by atomic layer deposition: The temperature dependence of residual stress, elastic modulus, hardness and adhesion, *Thin Solid Films*, 2014, **552**, 124–135.

47 M. Mattinen, J. Hämäläinen, F. Gao, P. Jalkanen, K. Mizohata, J. Räisänen, R. L. Puurunen, M. Ritala and M. Leskelä, Nucleation and Conformality of Iridium and Iridium Oxide Thin Films Grown by Atomic Layer Deposition, *Langmuir*, 2016, **32**, 10559–10569.

48 ALD saturation profile - open data, https://zenodo.org/communities/ald-saturation-profile-open-data/, (accessed July 14, 2021).

778 49 A. Yanguas-Gil and W. E. Jeffrey, machball, https://github.com/aldsim/machball, (accessed
779 July 14, 2021).

780 50 P. Atkins and J. de Paula, *ATKINS' PHYSICAL CHEMISTRY*, Oxford University Press, 8th edn.,
781 2006.

Supporting information

Conformality of atomic layer deposition in microchannels: impact of process parameters on the simulated thickness profile

Authors: Jihong Yim,[1]* Emma Verkama,[1]* Jorge A. Velasco,[1] Karsten Arts,[2] and Riikka L. Puurunen[1]**

*These authors contributed equally

** Corresponding author: riikka.puurunen@aalto.fi

[1]Department of Chemical and Metallurgical Engineering, Aalto University, P.O. Box 16100 (Kemistintie 1, Espoo), FI-00076 AALTO, Finland

[2]Department of Applied Physics, Eindhoven University of Technology, P.O. Box 513, 5600 MB Eindhoven, The Netherlands

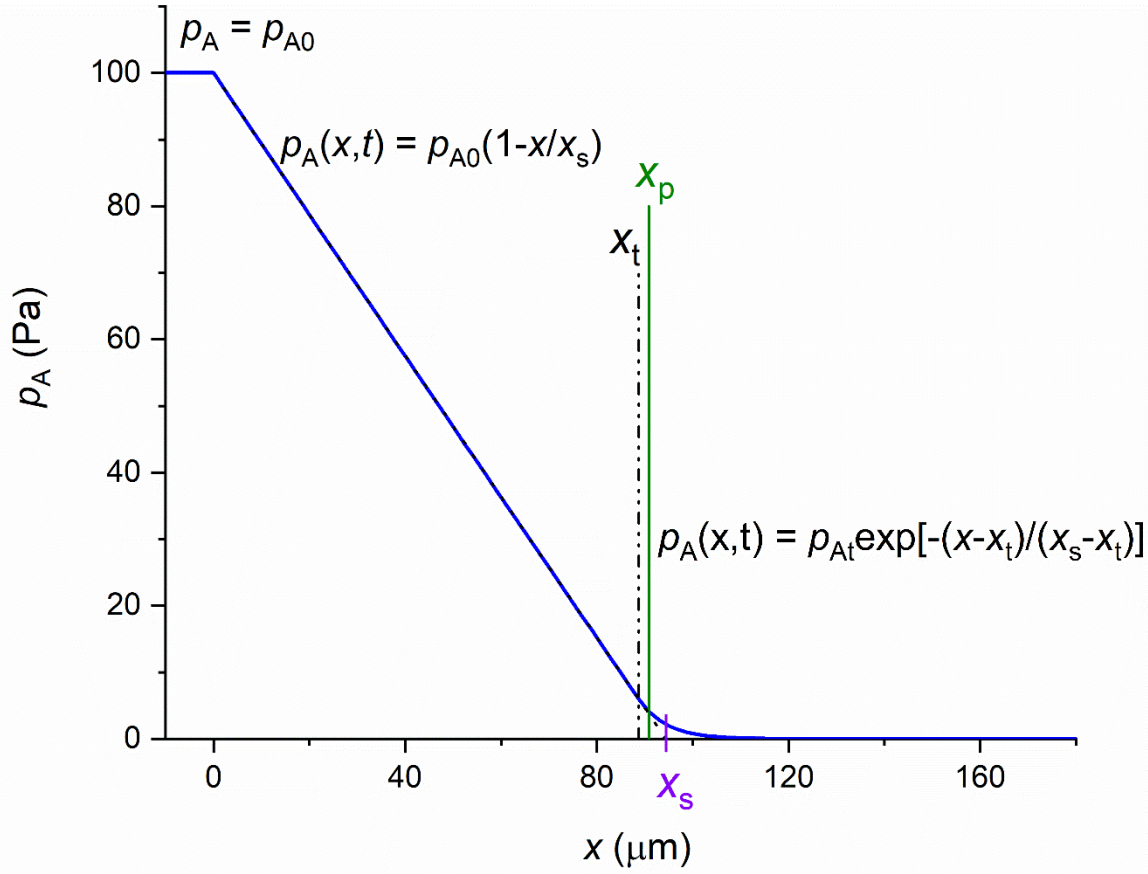

Figure S 1. Distribution of the partial pressure of Reactant A within the distance x. When $x < x_t$, partial pressure of Reactant A decreases linearly (Eq. 8). Linearly extrapolated partial pressure becomes zero at x_s (Eq. 10). When $x > x_t$, different simplification is used to describe the partial pressure (Eq. 9) within the distance. Half-thickness penetration depth is expressed as x_p.

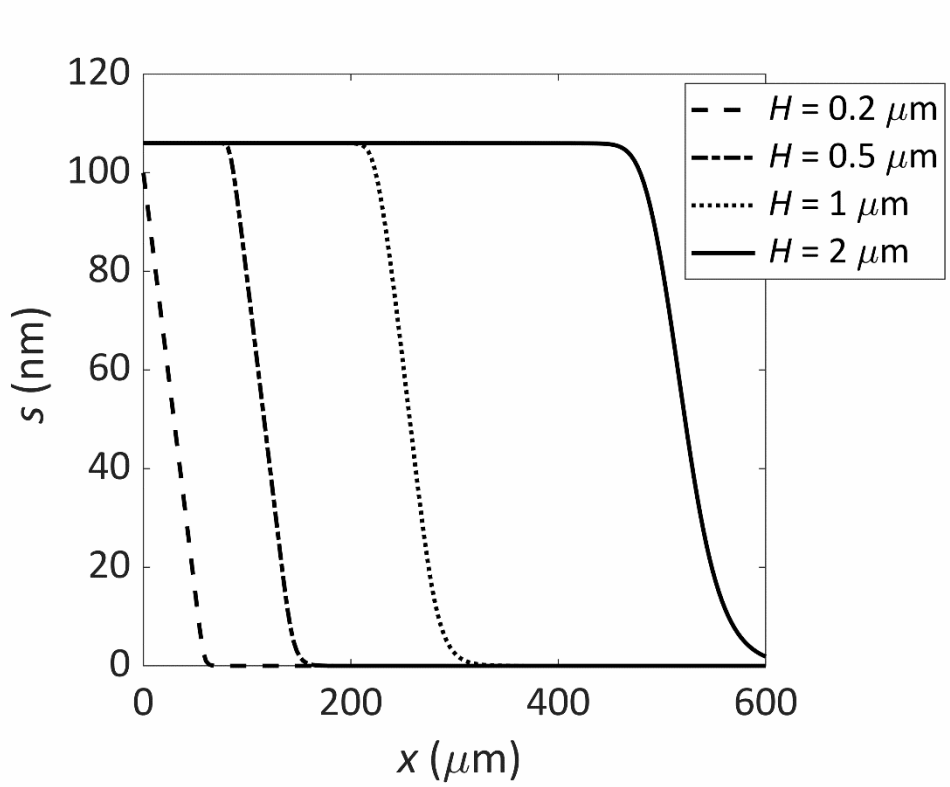

Figure S 2. Effect of channel height H on ALD thickness profile after 1000 cycles was simulated by MATLAB by using the parameter values applied to obtain Fig 4. from Ylilammi et al.[1] Parameter values used: W = 0.1 mm, p_{A0} = 100 Pa, M_A = 0.0749 kg mol^{-1}, d_A = 5.91 × 10^{-10} m, M_I = 0.028 kg mol^{-1}, d_I = 3.74 × 10^{-10} m, p_I = 300 Pa, q = 5 × 10^{18} m^{-2}, T = 500 K, K = 100 Pa^{-1}, c = 0.01, and gpc_{sat} = 1.06 × 10^{-10} m.

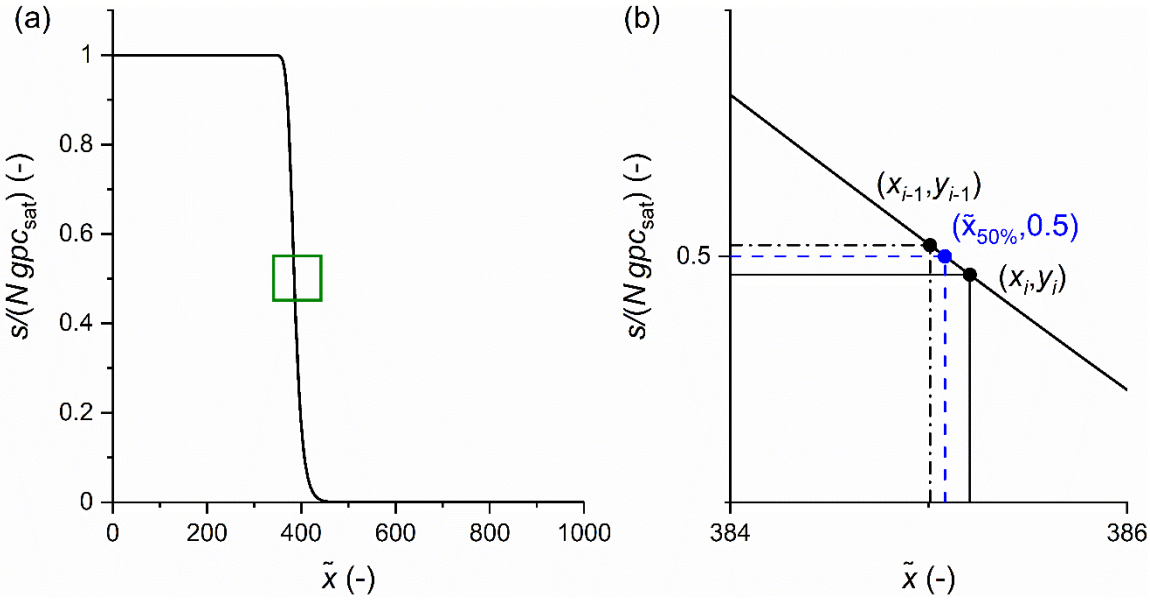

Figure S 3. (a) Example of Type 1 normalized thickness profile. (b) Details of the part of panel (a) marked with a green box. Half-thickness penetration depth $\tilde{x}_{50\%}$ and slope at half-thickness penetration depth are interpolated linearly between points (x_i,y_i), where x_i equal to or smaller than half-thickness penetration depth, and (x_{i-1},y_{i-1}).

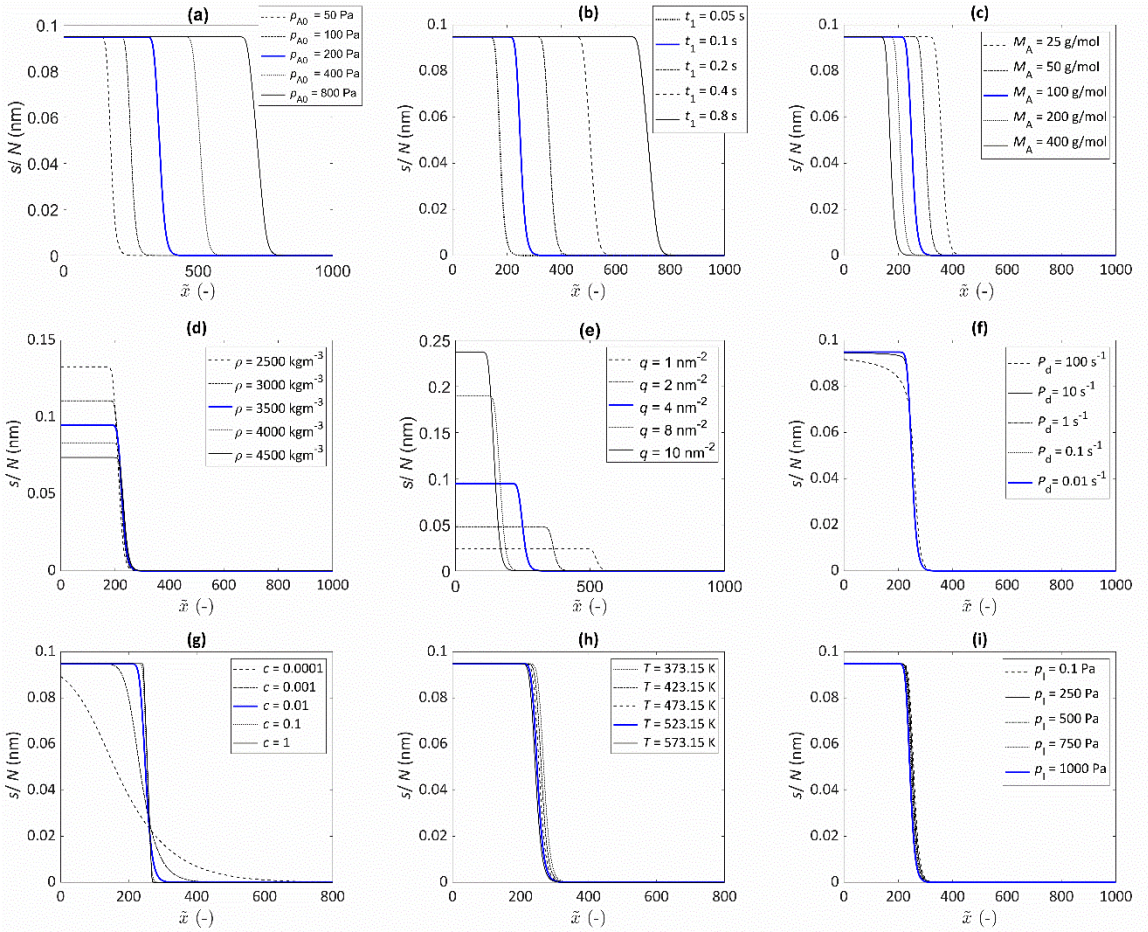

Figure S 4. Illustration of the effect of varying individual parameters on the scaled thickness profile in microchannels, simulated with the Ylilammi et al.[1] model re-implemented in this work. The parameter values used in the simulation are presented in Table 1; the simulation with the baseline values is shown as a solid blue line. The effect of (a) initial partial pressure of the Reactant A p_{A0}, (b) pulse length of Reactant A t_1, (c) molecular mass of Reactant A M_A, (d) film density ρ, (e) adsorption capacity q, (f) desorption probability P_d, (g) (lumped) sticking coefficient c, (h) ALD process temperature T, and (i) inert gas pressure p_I.

Table S 1. The fraction of channel filled depending on varied original channel height *H* with 250 cycles and varied number of cycles *N* within the original channel height of 500 nm, half-thickness penetration depth $\tilde{x}_{50\%}$ (-) and absolute value of the slope at $\tilde{x}_{50\%}$ (-) of scaled thickness profile.*

***H* (nm)**	***N* (-)**	**Fraction of channel filled (-)**	$\tilde{\boldsymbol{x}}_{\mathbf{50\%}}$ **(-)**	$\lvert d(s/N)/d\tilde{x}\rvert_{\tilde{x}_{50\%}}(-)$	***Kn* (-)**
100	250	0.4744	206.1	0.0007	38
200	250	0.2372	236.4	0.0015	19
500	250	0.0949	250.1	0.0026	8
1000	250	0.0474	248.8	0.0030	4
2000	250	0.0237	238.7	0.0032	2
2500	250	0.0190	233.5	0.0033	2
4000	250	0.0119	219.1	0.0035	1
500	**5**	0.0019	261.5	0.0029	8
500	**10**	0.0038	261.3	0.0029	8
500	**20**	0.0076	260.8	0.0030	8
500	**50**	0.0190	259.4	0.0029	8
500	**100**	0.0380	257.0	0.0029	8
500	**250**	0.0950	250.1	0.0026	8
500	**500**	0.1898	238.5	0.0018	8

**To satisfy the criteria of a difference between the two discretisation points in the y-axis below 3% out of the whole range, 1500 discretisation points were used for the simulation with the varied original channel height from 100 to 1000 nm and varied number of cycles. 2800 discretisation points were used for the simulation with the original channel height over 1000 nm.*

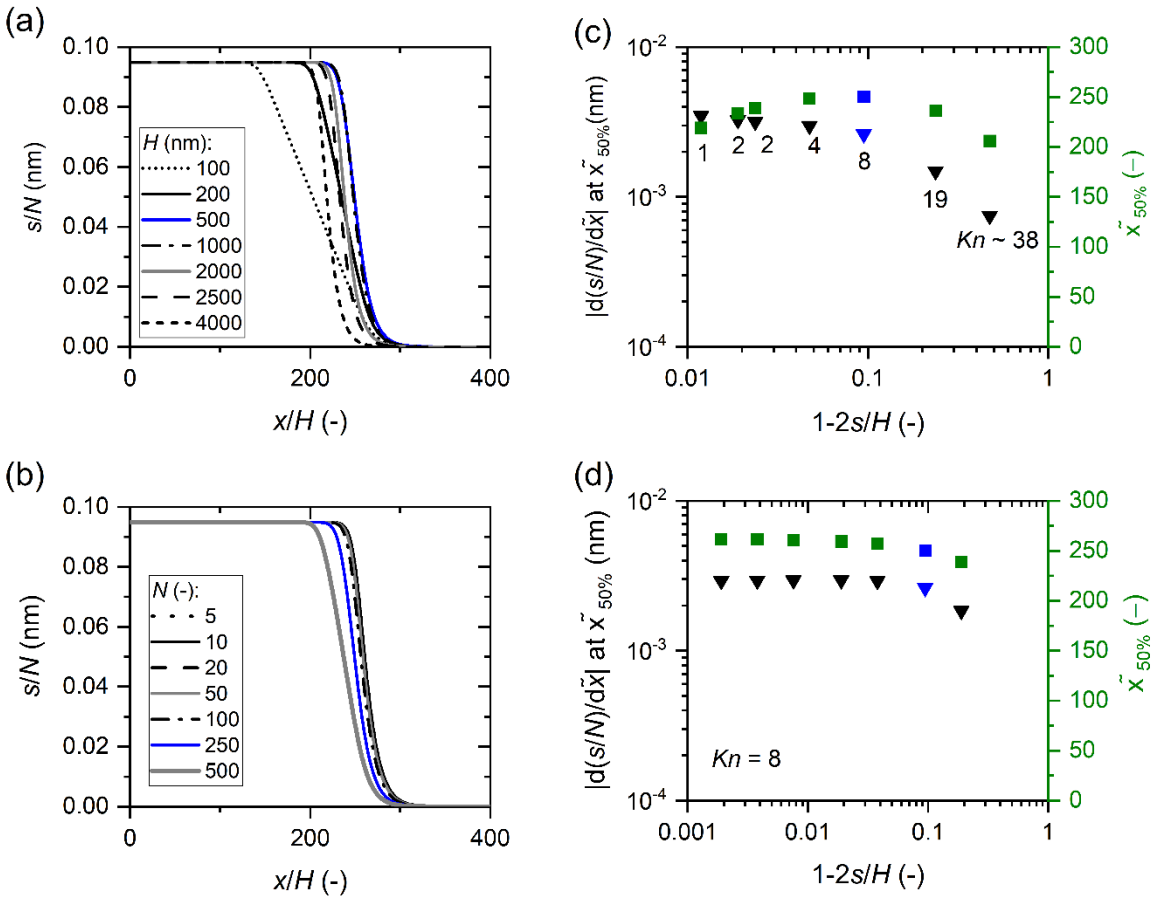

Figure S 5. Scaled thickness profile with (a) varying original channel height H with 250 cycles and (b) varying number of cycles N within the original channel height of 500 nm. (c) Half-thickness penetration depth $\tilde{x}_{50\%}\ (-)$ and absolute value of the slope at $\tilde{x}_{50\%}$ of the scaled thickness profile in panel (a) against the fraction of channel filled. (d) Half-thickness penetration depth $\tilde{x}_{50\%}\ (-)$ and absolute value of the slope at $\tilde{x}_{50\%}\ (-)$ of the scaled thickness profile in panel (b) against the fraction of channel filled. Knudsen number was calculated for each case. Simulation results with baseline condition is marked in blue.

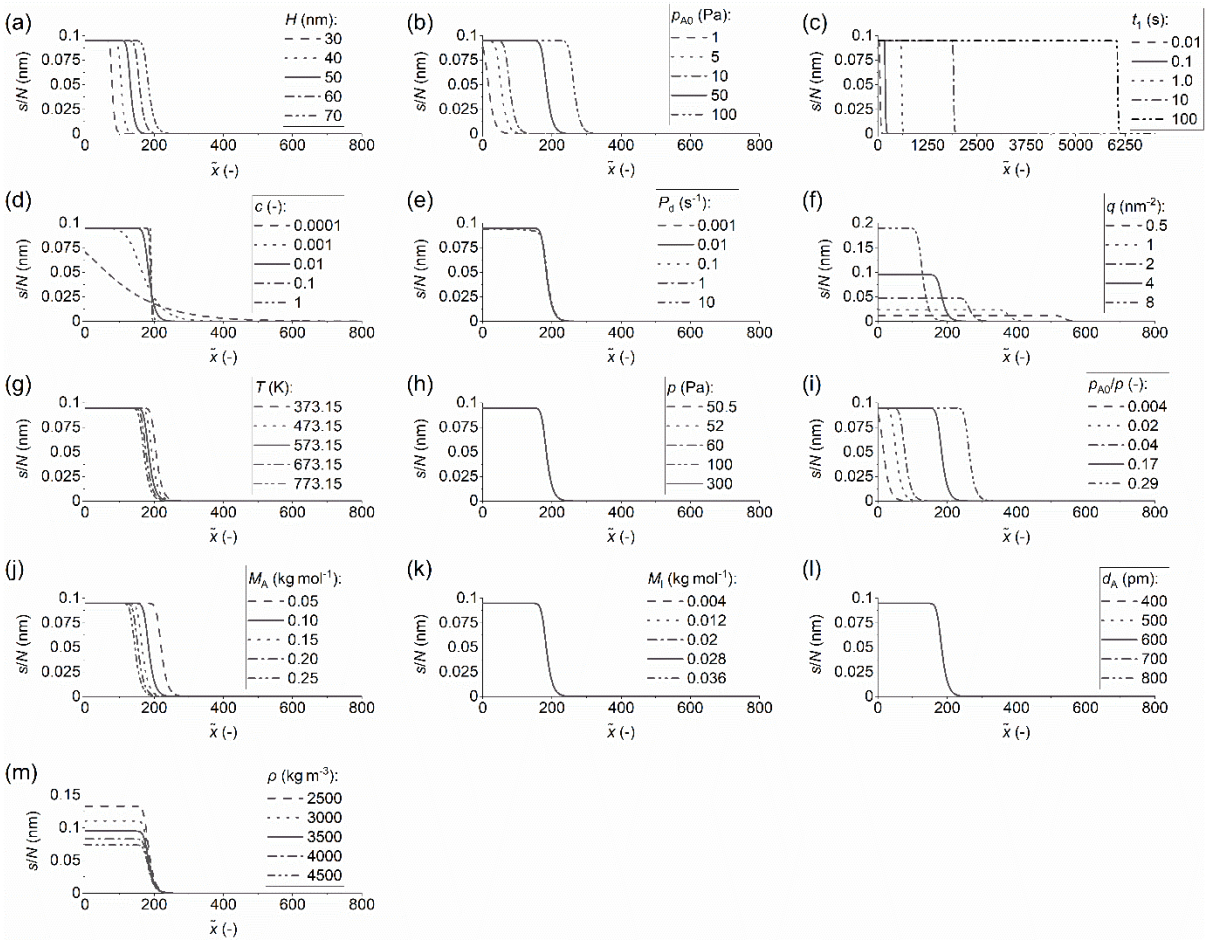

Figure S 6. Scaled thickness profiles simulated in free molecular flow regime (*Kn* >> 1) by implementing Ylilammi et al.[1] model with varying (a) original channel height, (b) initial partial pressure of Reactant A, (c) pulse length, (d) (lumped) sticking coefficient, (e) desorption probability, (f) adsorption density, (g) temperature, (h) total pressure, (i) ratio between initial partial pressure of Reactant A to total pressure, (j) molar mass of Reactant A, (K) molar mass of inert gas, (l) diameter of Reactant A, and (m) film density. Parameter values used, if otherwise stated: $H = 5 \times 10^{-8}$ m, $N = 1$, $t_1 = 0.1$ s, $p_{A0} = 50$ Pa, $M_A = 0.1$ kg mol^{-1}, $d_A = 6.0 \times 10^{-10}$ m, $M_I = 0.028$ kg mol^{-1}, $d_I = 4.0 \times 10^{-10}$ m, $p_I = 250$ Pa, $q = 4 \times 10^{18}$ m^{-2}, $\rho = 3500$ kg m^{-3}, $M = 0.050$ kg mol^{-1}, $P_d = 0.01$ s^{-1}, and $c = 0.01$.

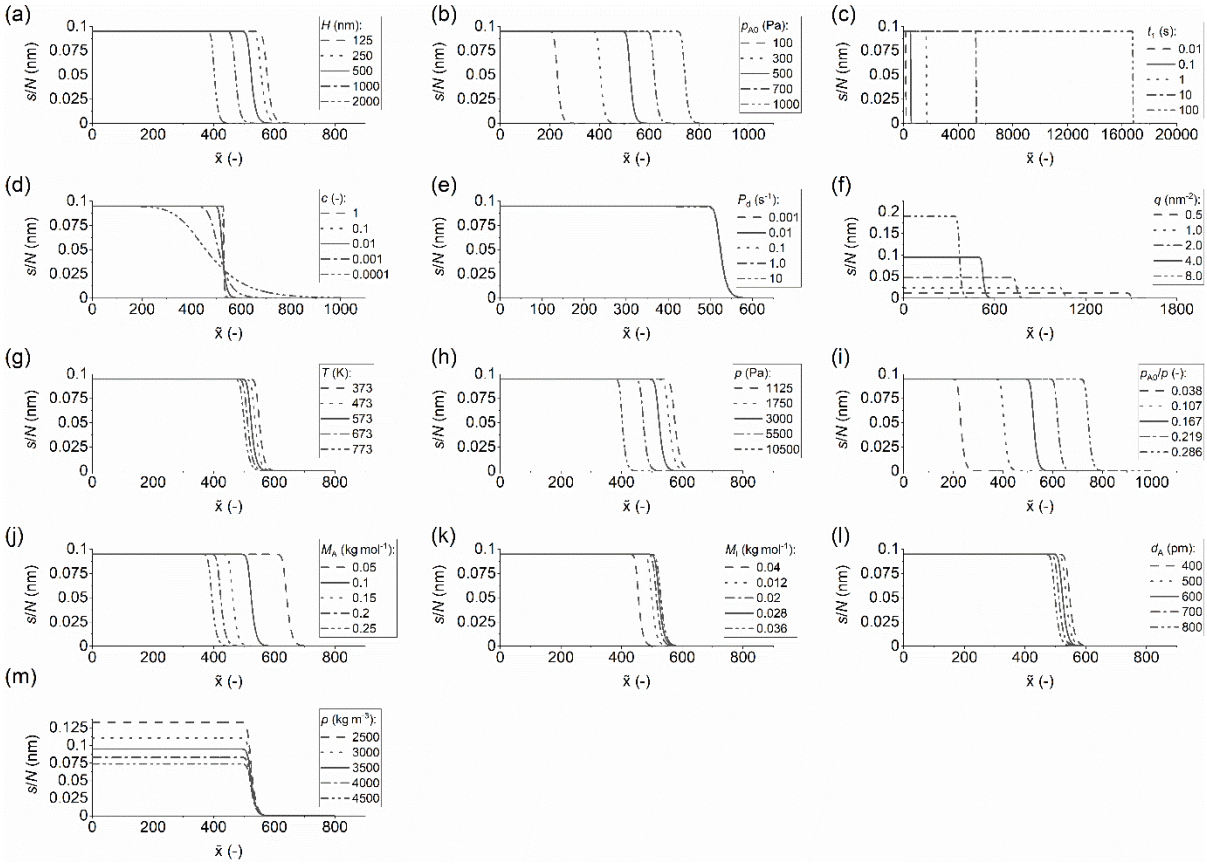

Figure S 7. Scaled thickness profiles simulated in transition flow regime ($Kn \approx 1$) by implementing Ylilammi et al.[1] model with varying (a) original channel height, (b) initial partial pressure of Reactant A, (c) pulse length, (d) (lumped) sticking coefficient, (e) desorption probability, (f) adsorption density, (g) temperature, (h) total pressure, (i) ratio between initial partial pressure of Reactant A to total pressure, (j) molar mass of Reactant A, (K) molar mass of inert gas, (l) diameter of Reactant A, and (m) film density. Parameter values used, if otherwise stated: $H = 5 \times 10^{-7}$ m, $N = 1$, $t_1 = 0.1$ s, $p_{A0} = 500$ Pa, $M_A = 0.1$ kg mol^{-1}, $d_A = 6.0 \times 10^{-10}$ m, $M_I = 0.028$ kg mol^{-1}, $d_I = 4.0 \times 10^{-10}$ m, $p_I = 2500$ Pa, $q = 4 \times 10^{18}$ m^{-2}, $\rho = 3500$ kg m^{-3}, $M = 0.050$ kg mol^{-1}, $P_d = 0.01$ s^{-1}, and $c = 0.01$.

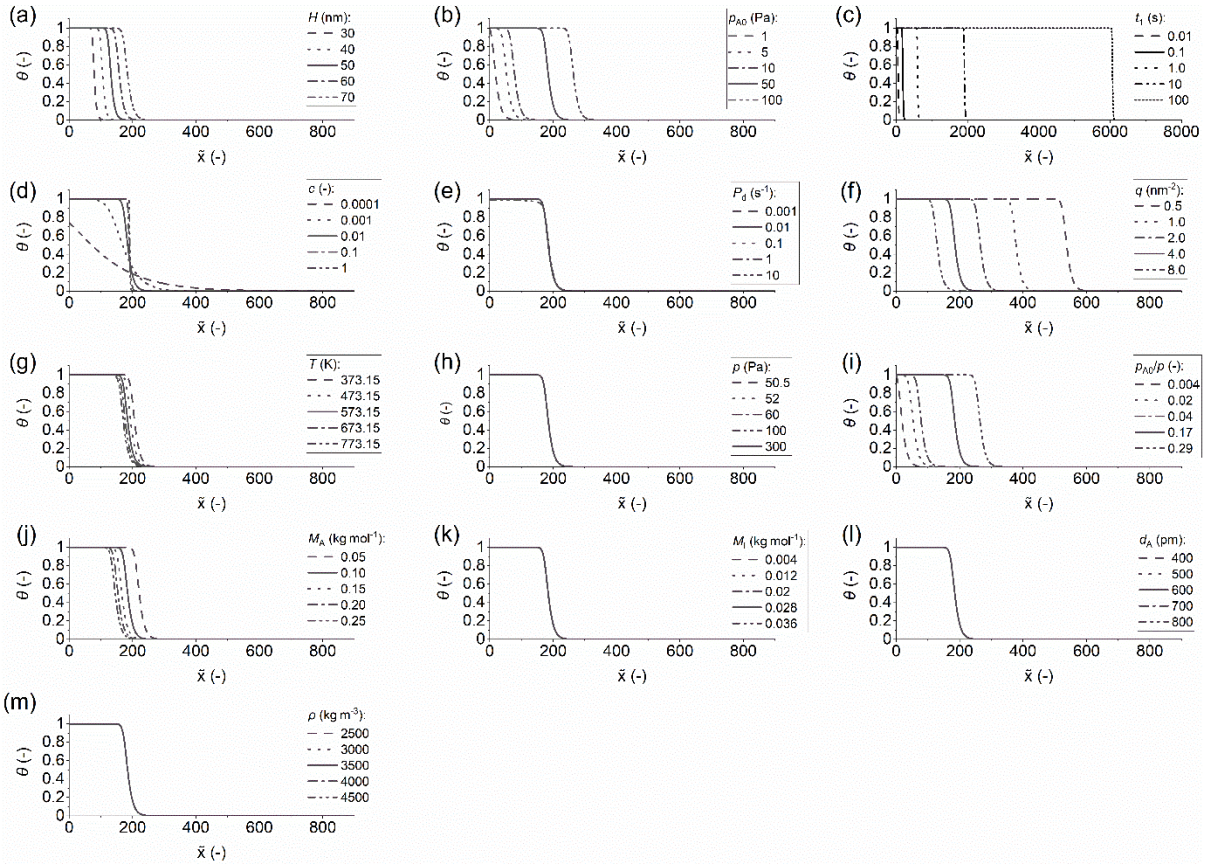

Figure S 8. Type 1 normalized thickness profiles simulated in free molecular flow regime (*Kn* >> 1) by implementing Ylilammi et al.[1] model with varying (a) original channel height, (b) initial partial pressure of Reactant A, (c) pulse length, (d) (lumped) sticking coefficient, (e) desorption probability, (f) adsorption density, (g) temperature, (h) total pressure, (i) ratio between initial partial pressure of Reactant A to total pressure, (j) molar mass of Reactant A, (K) molar mass of inert gas, (l) diameter of Reactant A, and (m) film density. Parameter values used, if otherwise stated: $H = 5 \times 10^{-8}$ m, $N = 1$, $t_1 = 0.1$ s, $p_{A0} = 50$ Pa, $M_A = 0.1$ kg mol^{-1}, $d_A = 6.0 \times 10^{-10}$ m, $M_I = 0.028$ kg mol^{-1}, $d_I = 4.0 \times 10^{-10}$ m, $p_I = 250$ Pa, $q = 4 \times 10^{18}$ m^{-2}, $\rho = 3500$ kg m^{-3}, $M = 0.050$ kg mol^{-1}, $P_d = 0.01$ s^{-1}, and $c = 0.01$.

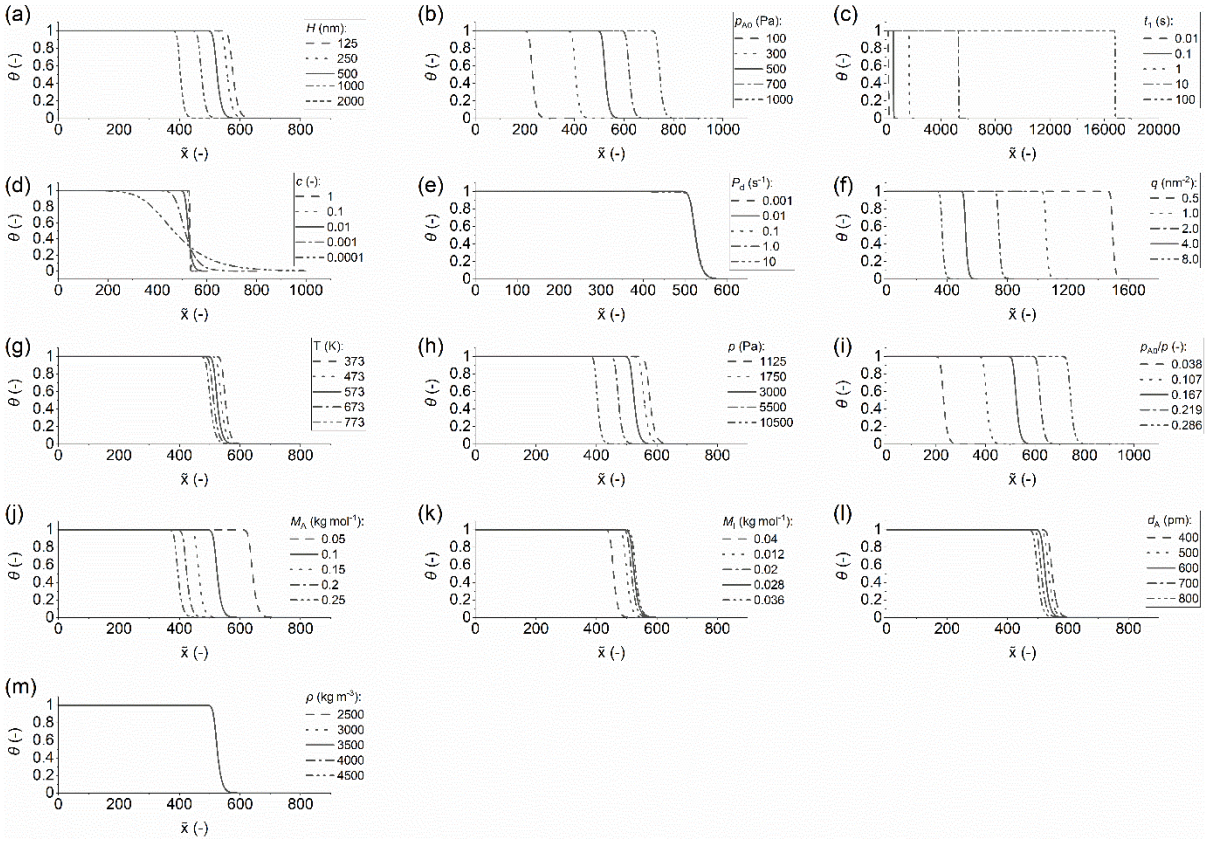

Figure S 9. Type 1 normalized thickness profiles simulated in transition flow regime (Kn ≈ 1) by implementing Ylilammi et al.[1] model with varying (a) original channel height, (b) initial partial pressure of Reactant A, (c) pulse length, (d) (lumped) sticking coefficient, (e) desorption probability, (f) adsorption density, (g) temperature, (h) total pressure, (i) ratio between initial partial pressure of Reactant A to total pressure, (j) molar mass of Reactant A, (K) molar mass of inert gas, (l) diameter of Reactant A, and (m) film density. Parameter values used, if otherwise stated: $H = 5 \times 10^{-7}$ m, $N = 1$, $t_1 = 0.1$ s, $p_{A0} = 500$ Pa, $M_A = 0.1$ kg mol^{-1}, $d_A = 6.0 \times 10^{-10}$ m, $M_I = 0.028$ kg mol^{-1}, $d_I = 4.0 \times 10^{-10}$ m, $p_I = 2500$ Pa, $q = 4 \times 10^{18}$ m^{-2}, $\rho = 3500$ kg m^{-3}, $M = 0.050$ kg mol^{-1}, $P_d = 0.01$ s^{-1}, and $c = 0.01$.

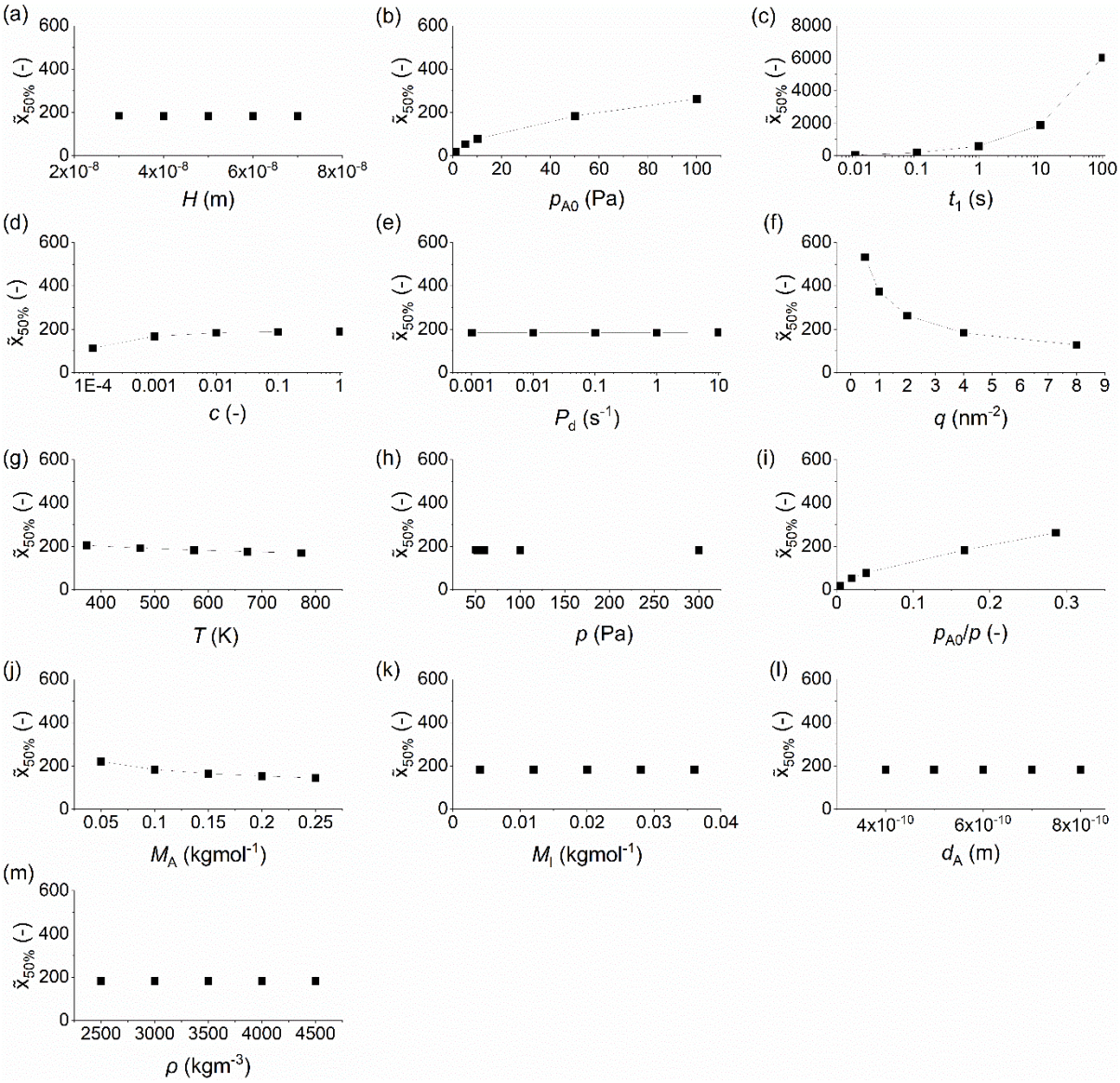

Figure S 10. Half-thickness penetration depth of scaled thickness profile simulated in free molecular flow regime (*Kn* >> 1) against varied parameters: (a) original channel height, (b) initial partial pressure of Reactant A, (c) pulse length, (d) (lumped) sticking coefficient, (e) desorption probability, (f) adsorption density, (g) temperature, (h) total pressure, (i) ratio between initial partial pressure of Reactant A to total pressure, (j) molar mass of Reactant A, (K) molar mass of inert gas, (l) diameter of Reactant A, and (m) film density. The scaled thickness profiles, on which this data is based, are in Figure S 6.

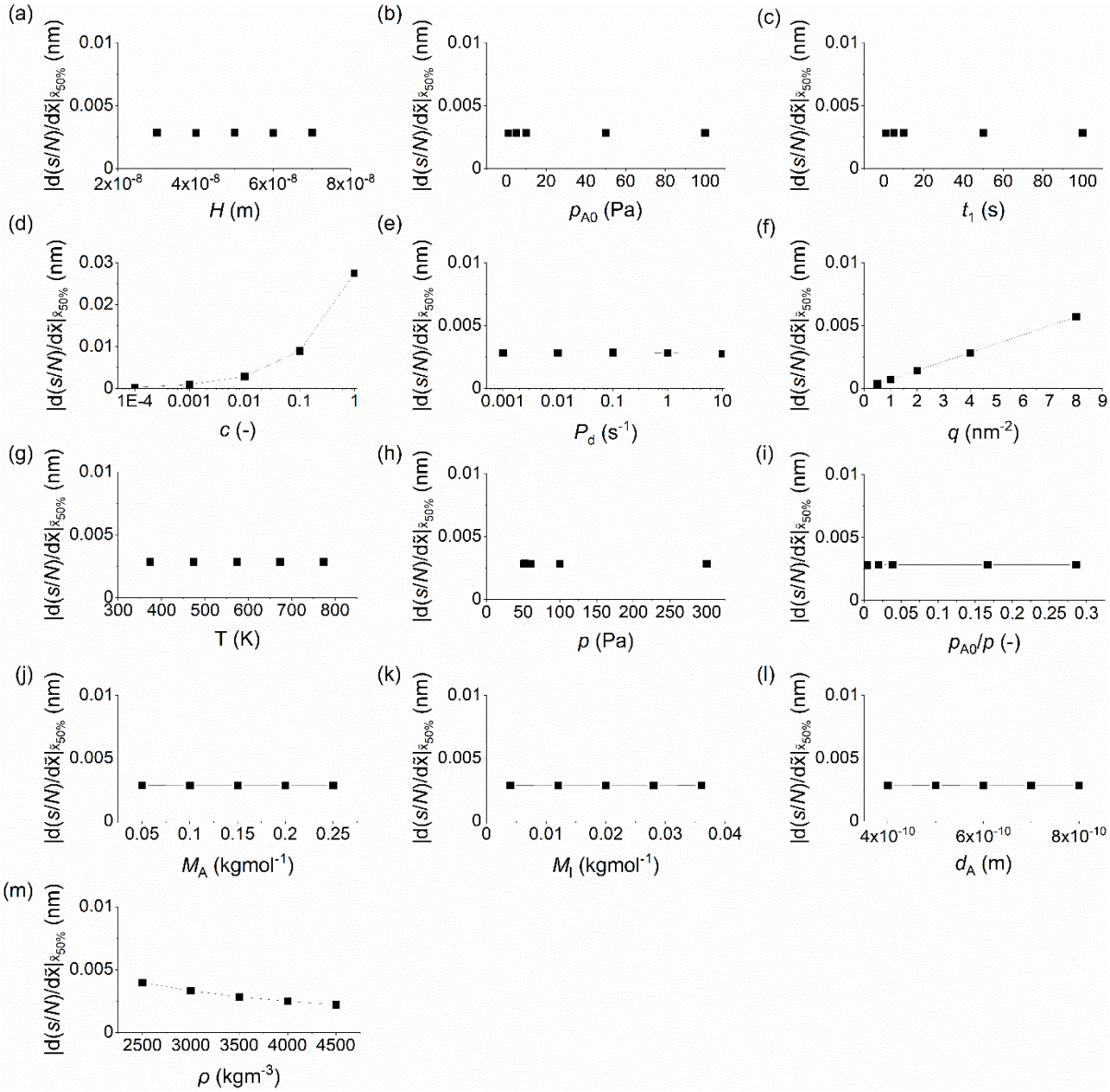

Figure S 11. Absolute value of the slope at half-thickness penetration depth of scaled thickness profile simulated in free molecular flow regime (*Kn* >> 1) against varied parameters: (a) original channel height, (b) initial partial pressure of Reactant A, (c) pulse length, (d) (lumped) sticking coefficient, (e) desorption probability, (f) adsorption density, (g) temperature, (h) total pressure, (i) ratio between initial partial pressure of Reactant A to total pressure, (j) molar mass of Reactant A, (K) molar mass of inert gas, (l) diameter of Reactant A, and (m) film density. The scaled thickness profiles, on which this data is based, are in Figure S 6.

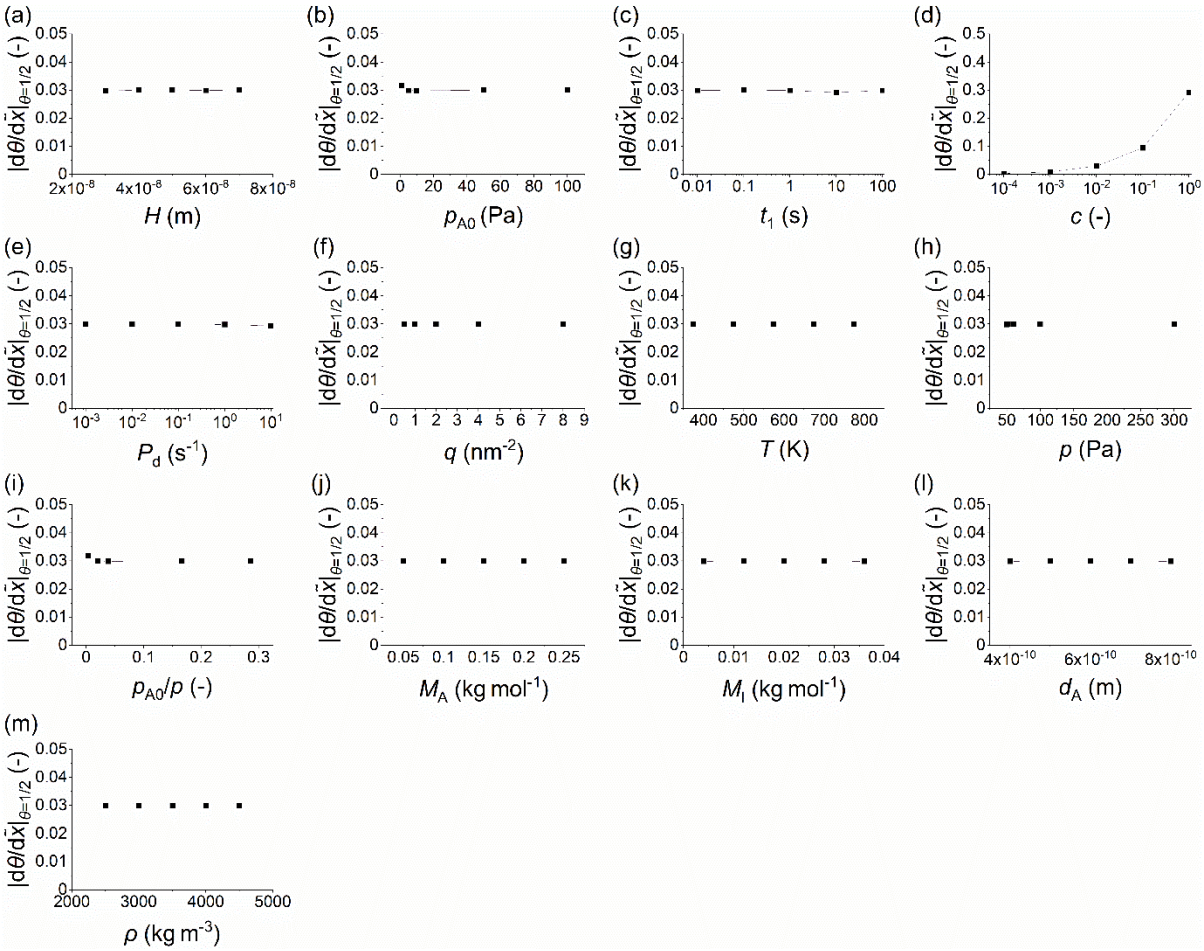

Figure S 12. Absolute value of the slope at half-thickness penetration depth of Type 1 normalized thickness profile simulated in free molecular flow regime (*Kn* >> 1) against varied parameters: (a) original channel height, (b) initial partial pressure of Reactant A, (c) pulse length, (d) (lumped) sticking coefficient, (e) desorption probability, (f) adsorption density, (g) temperature, (h) total pressure, (i) ratio between initial partial pressure of Reactant A to total pressure, (j) molar mass of Reactant A, (K) molar mass of inert gas, (l) diameter of Reactant A, and (m) film density. The Type1 normalized thickness profiles, on which this data is based, are in Figure S 8.

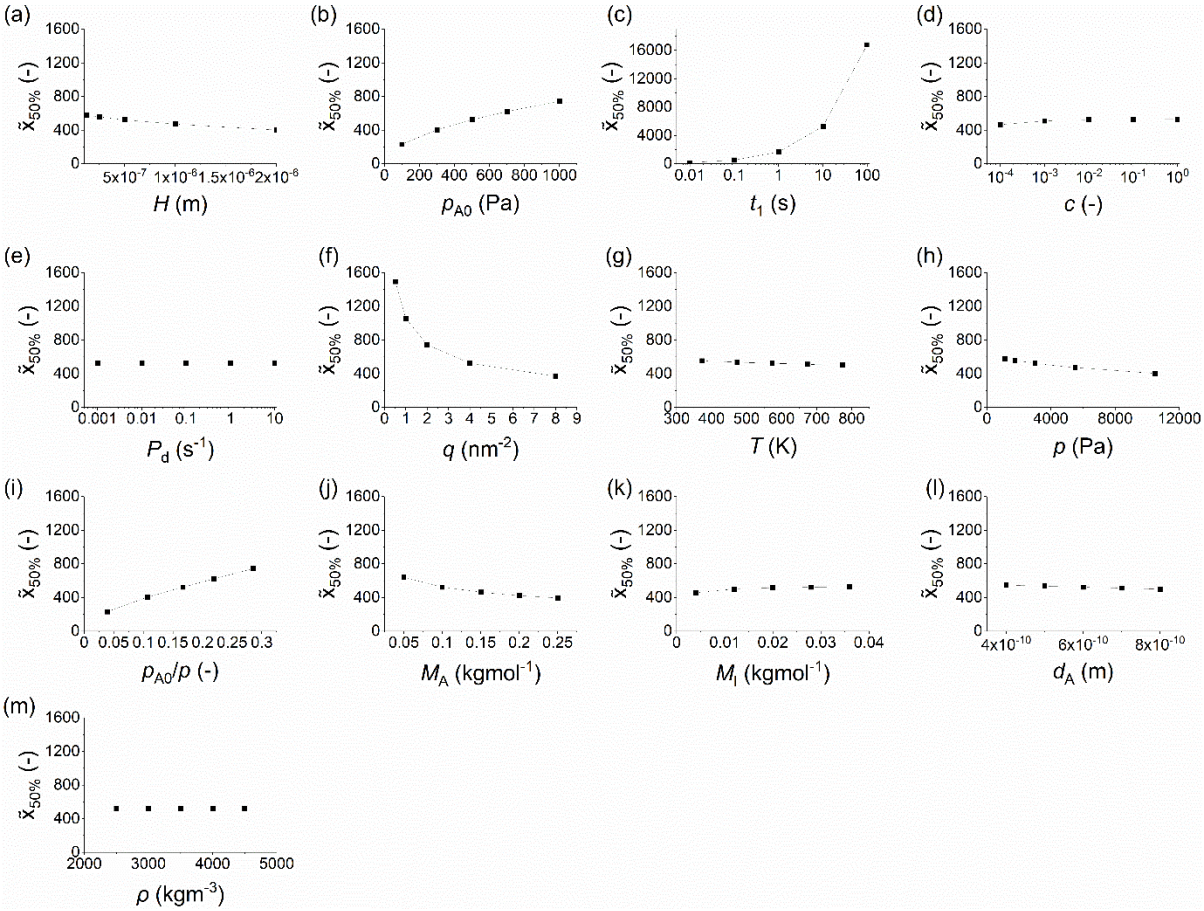

Figure S 13. Half-thickness penetration depth of scaled thickness profile simulated in transition flow regime ($Kn \approx 1$) against varied parameters: (a) original channel height, (b) initial partial pressure of Reactant A, (c) pulse length, (d) (lumped) sticking coefficient, (e) desorption probability, (f) adsorption density, (g) temperature, (h) total pressure, (i) ratio between initial partial pressure of Reactant A to total pressure, (j) molar mass of Reactant A, (K) molar mass of inert gas, (l) diameter of Reactant A, and (m) film density. The scaled thickness profiles, on which this data is based, are in Figure S 7.

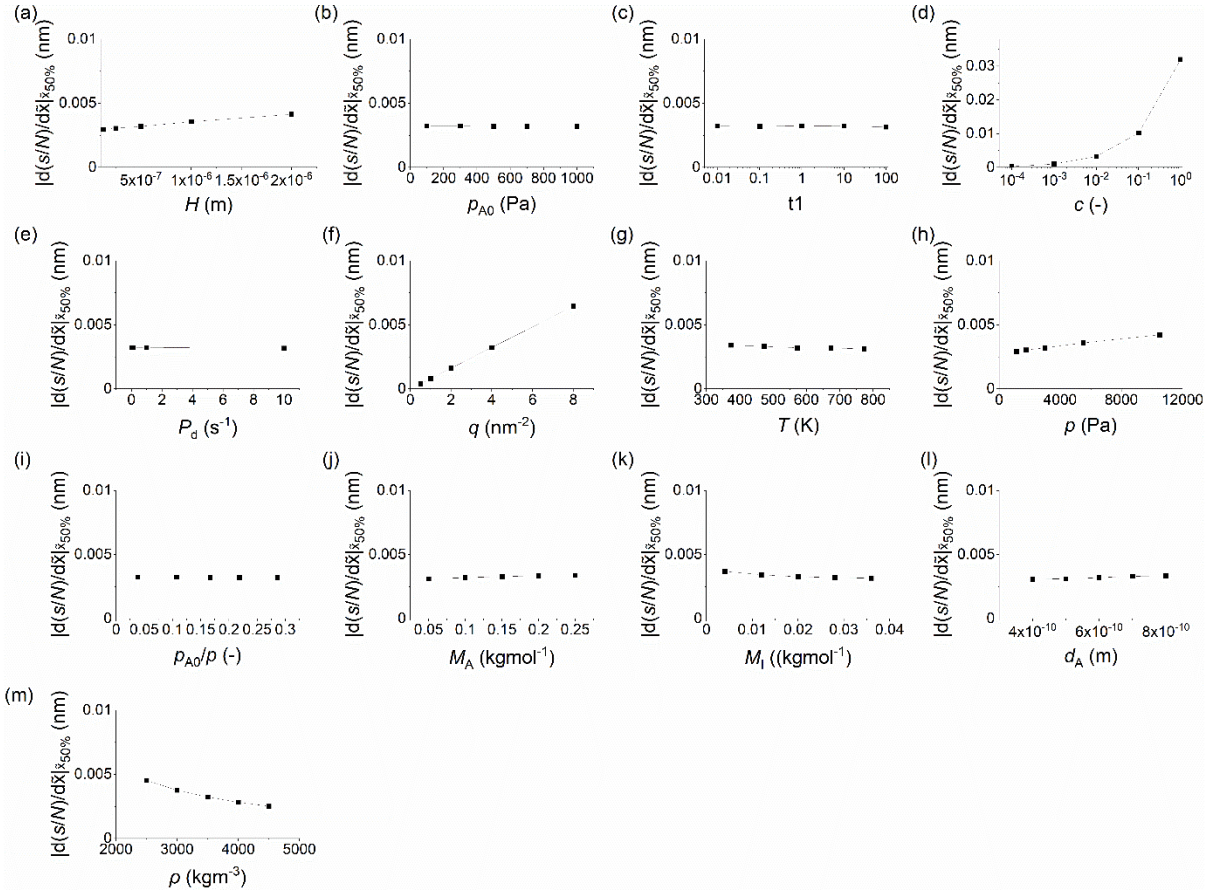

Figure S 14. Absolute value of the slope at half-thickness penetration depth of scaled thickness profile simulated in transition flow regime ($Kn \approx 1$) against varied parameters: (a) original channel height, (b) initial partial pressure of Reactant A, (c) pulse length, (d) (lumped) sticking coefficient, (e) desorption probability, (f) adsorption density, (g) temperature, (h) total pressure, (i) ratio between initial partial pressure of Reactant A to total pressure, (j) molar mass of Reactant A, (K) molar mass of inert gas, (l) diameter of Reactant A, and (m) film density. The scaled thickness profiles, on which this data is based, are in Figure S 7.

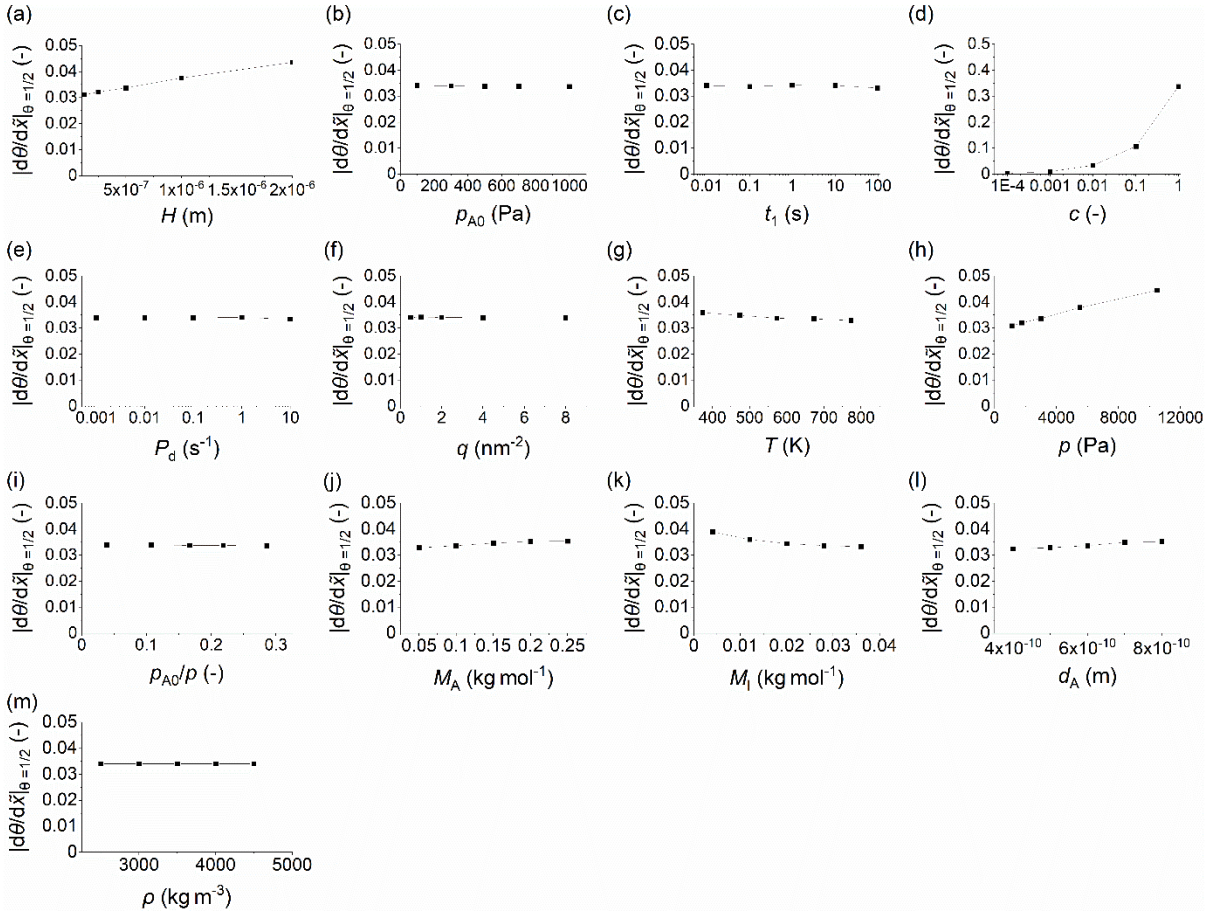

Figure S 15. Absolute value of the slope at half-thickness penetration depth of Type 1 normalized thickness profile simulated in transition flow regime ($Kn \approx 1$) against varied parameters: (a) original channel height, (b) initial partial pressure of Reactant A, (c) pulse length, (d) (lumped) sticking coefficient, (e) desorption probability, (f) adsorption density, (g) temperature, (h) total pressure, (i) ratio between initial partial pressure of Reactant A to total pressure, (j) molar mass of Reactant A, (K) molar mass of inert gas, (l) diameter of Reactant A, and (m) film density. The Type 1 normalized thickness profiles, on which this data is based, are in Figure S 9.

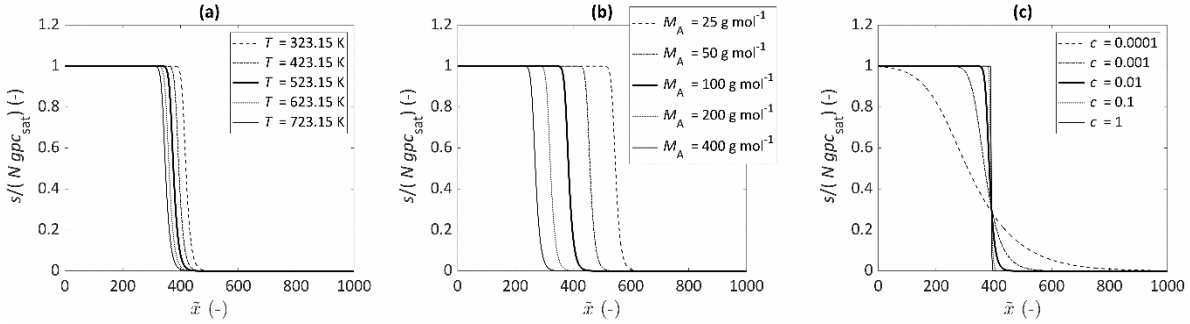

Figure S 16. Type 1 normalized thickness profiles simulated in a wide microchannel in free molecular flow with varying (a) different process temperature, (b) molar mass of reactant A, and (c) sticking coefficient. Sticking coefficient values back-extracted from these thickness profiles by the slope method[2] are listed in Table 3. Parameters used if not otherwise stated: H = 200 nm, N =1, W = 10 mm, T = 523.15 K, t_1 = 2 s, p_{A0} = 10 Pa, M_A = 0.1 kg mol^{-1}, d_A = 600 pm, M_I = 0.028 kg mol^{-1}, d_I = 374 pm, p_I = 50 Pa, q = 4×10^{18} m^{-2}, ρ = 3500 kg m^{-3}, M = 0.050 kg mol^{-1}, P_d = 10^{-5} s^{-1}, and c = 0.01.

References

1 M. Ylilammi, O. M. E. Ylivaara and R. L. Puurunen, Modeling growth kinetics of thin films made by atomic layer deposition in lateral high-aspect-ratio structures, *Journal of Applied Physics*, 2018, **123**, 205301. https://doi.org/10.1063/1.5028178

2 K. Arts, V. Vandalon, R. L. Puurunen, M. Utriainen, F. Gao, W. M. M. Kessels and H. C. M. Knoops, Sticking probabilities of H2O and Al(CH3)3 during atomic layer deposition of Al2O3 extracted from their impact on film conformality, *Journal of Vacuum Science & Technology A*, 2019, **37**, 030908. https://doi.org/10.1116/1.5093620